D4.4 RISK MANAGEMENT

Kenneth Gavin, Cormac Reale, Kevin Duffy and Aryan Gupta,
InGEO

@AshvinH2020
ASHVIN H2020 Project
www.ashvin.eu

ASHVIN has received funding from the European Union's Horizon 2020 research and innovation programme under Grant Agreement No 958161. This document reflects only the author's view and the Commission is not responsible for any use that may be made of the information it contains.

Project Title	Assistants for Healthy, Safe, and Productive Virtual Construction Design, Operation & Maintenance using a Digital Twin
Project Acronym	ASHVIN
Grant Agreement No	958161
Instrument	Research & Innovation Action
Topic	LC-EEB-08-2020 - Digital Building Twins
Start Date of Project	1st October 2020
Duration of Project	36 Months

Name of the deliverable	Risk Management
Number of the deliverable	D4.4
Related WP number and name	WP 4 Control and real-time simulation of construction
Related task number and name	T4.4 Data driven risk management
Deliverable dissemination level	PU
Deliverable due date	31-12-2022
Deliverable submission date	31-12-2022
Task leader/Main author	Kenneth Gavin (InGEO)
Contributing partners	Cormac Reale, Kevin Duffy and Aryan Gupta (InGEO)
Reviewer(s)	

ABSTRACT

In order to develop comprehensive digital-twin supported site risk management regime it is important to collect data on productivity from well-documented previous construction activities. One of the highest risk activities in construction relates to unknown or unanticipated soil conditions. Soils are naturally occurring, variable materials whose properties depend on stress and strain level and vary temporally. Current design methods deal with uncertainty by assuming conservative estimates of soil properties and calculating the response of the geotechnical structure to some unlikely set of extreme loads. In certain analyses involving soil-structure interaction problems (e.g. soil retaining structures) the loads experienced by structural elements (such as piles, anchors, walls etc.) are directly related to the displacements (strains) experienced. Therefore, only a model that uses the most-likely soil and structure properties at any given point in the life-cycle of a structure to accurately predict the displacement can allow the real safety level (resistance to additional loading) of a structure to be determined.

This deliverable uses monitoring data collected from the construction of a deep sea quay wall to determine the real safety level of the wall throughout the construction programme. An advanced finite element model is implemented that can capture the real response. By comparing the measured and predicted response of the wall, a number of updates are initiated that incorporate the knowledge gathered and allow for reduction of uncertainty in a logical and consistent manner. The development of Ports is driven by ever increasing vessel sizes. To replace an existing quay wall to allow for larger vessels means an investment of several 100 million euros and a significant environmental cost in terms of CO_2 emissions from new construction. In this report the digital twin developed demonstrated the safety level of the existing wall to several metres of additional dredging.

KEYWORDS

Digital Twin, Quay Wall, Finite Element Model, Updating, Soil Properties, Safety Level

REVISIONS

Version	Submission date	Comments	Author
V0.1	30/12/2022		KGG
V0.2	26/05/2022	Review comments addressed.	KGG
V0.3	04/06/2022	Final	KGG
……			
…….			

DISCLAIMER

ACRONYMS & DEFINITIONS

R	Capacity of a structure
D	Demand; load on a structure
N.A.P.	Normal Amsterdam Level
CPT	Cone Penetration Testing
q_c	The cone end resistance measured in CPT test
f_s	The sleeve friction measured in CPT test
u_2	The pore water pressure measured in CPT test
v_s.	The shear wave modulus of soil
F_r	The friction ratio, $F_r = f_s/q_c$
SBT	Soil Behaviour Type
I_c	Soil behaviour type index
γ	Unit weight of soil
γ_w	Unit weight of water
q_t	Corrected cone resistance
σ_{vo} , σ'_{vo}	Total and effective vertical stress respectively
P_{atm}	Atmospheric pressure
HS, HSS	Hardening Soil model, Hardening Soil Small-strain model
σ'_p	Past maximum vertical effective stress
OCR	Over consolidation ratio
K_0	Lateral earth pressure coefficient at rest
D_r	Density
$E_{50,ref}$	Reference secant stiffness in standard drained triaxial test
$E_{oed,ref}$	Reference tangent stiffness for primary oedometer loading
$E_{ur,ref}$	Reference unloading/reloading stiffness
$G_{0,ref}$	Reference small-strain shear modulus
SI Pile	Screw Injection type pile
MV Pile	Grouted anchor I section pile
D	Outside diameter of open-ended pile
t	Wall thickness of open-ended pile
W	Width of sheet pile
H	Depth of sheet pile

D_s	Diameter of the shaft of an SI Pile
D_b	Diameter of the base of an SI Pile
τ_f	Unit pile shaft resistance
q_b	Unit pile base resistance
q_{st}	Unit shaft resistance developed by a tension anchor
α_s, α_p, α_t	Reduction factor used for the shaft resistance of an SI pile, base resistance of an SI pile and tension shaft resistance of grouted anchors respectively
FBG	Fibre Bragg Grating
BOFDA	Brillouin Optical Frequency Domain Analysis

ASHVIN PROJECT

ASHVIN aims at enabling the European construction industry to significantly improve its productivity, while reducing cost and ensuring absolutely safe work conditions, by providing a proposal for a European wide digital twin standard, an open source digital twin platform integrating IoT and image technologies, and a set of tools and demonstrated procedures to apply the platform and the standard proven to guarantee specified productivity, cost, and safety improvements. The envisioned platform will provide a digital representation of the construction product at hand and allow to collect real-time digital data before, during, and after production of the product to continuously monitor changes in the environment and within the production process. Based on the platform, ASHVIN will develop and demonstrate applications that use the digital twin data. These applications will allow it to fully leverage the potential of the IoT based digital twin platform to reach the expected impacts (better scheduling forecast by 20%; better allocation of resources and optimization of equipment usage; reduced number of accidents; reduction of construction projects). The ASHVIN solutions will overcome worker protection and privacy issues that come with the tracking of construction activities, provide means to fuse video data and sensor data, integrate geo-monitoring data, provide multi-physics simulation methods for digital representing the behavior of a product (not only its shape), provide evidence based engineering methods to design for productivity and safety, provide 4D simulation and visualization methods of construction processes, and develop a lean planning process supported by real-time data. All innovations will be demonstrated on real-world construction projects across Europe. The ASHVIN consortium combines strong R&I players from 9 EU member states with strong expertise in construction and engineering management, digital twin technology, IoT, and data security / privacy.

TABLE OF CONTENTS

INDEX OF FIGURES

INDEX OF TABLES

1 INTRODUCTION

In task 4.4 a comprehensive digital-twin supported construction site management regime will be considered. The digital twin was envisaged to be based on detailed data collected for a past construction project. The focus was to develop advanced risk management regimes related to soil related risks and risk related to temporary structural site conditions – leveraging the full power of an adequate real-time digital representation of the construction product during production. This was achieved through the fused data collected in Task 3.3 and Task 3.4 of the ASHVIN project. This data was used towards the following objectives:

(i) Create a probabilistic ground model that formed the basis of an advanced finite element model (FEM) of a complex quay wall construction project.
(ii) The embedded sensor data collected at the site was used to refine constitutive models and the respective input parameters to reduce uncertainties in soil properties including strength and stiffness.
(iii) These FEM models can then be used to run what-if scenarios to determine the impact of changes in the construction sequence, time etc. and in response to queries from the client, calculate the real safety level of the structure and the possibility of extending its deign life.

After introducing the rationale for using digital twins for the management of risk for quay wall structures a case study of the performance of a deep sea quay wall during the construction stage is presented that achieves the objectives described in (i) to (iiii) above.

This report draws heavily on the data sources outlined in Deliverable 3.2 - Digital Twin based Geo-Monitoring of the ASHVIN project. Specifically multiple data sources were used to determine the ground model at the site. The wall was continuously monitored throughout the construction process using embedded sensors that allowed the structural response to be determined during all construction phases. This data allowed for model updating and refinement. Stress tests performed with this calibrated model gave good confidence on the operational safety level of the structure and allowed various scenarios for reuse of the structure to be determined in order for the asset owner to consider the flexibility of the structure.

2 WHY USE DIGITAL TWINS FOR RISK MANAGEMENT OF DEEP EXCAVATIONS

Engineers generally use prescriptive design codes to manage risk by adopting conservative estimates of the properties of the materials used and comparing their performance to some extreme loading scenario. Unlike branches of civil engineering like structural engineering, where the strength and stiffness properties of the material e.g. steel or concrete can be specified by the designer, and rigorous quality control procedures can ensure reliability, geotechnical engineering has added complexities.

2.1 Natural Variability

Soil is a naturally occurring material with properties that vary spatially (in both horizontal and vertical directions), change with stress and strain level and are influenced by environmental factors such as water content and temperature. An example of the natural variability of soil is evident in Figure 1 that shows the geological profile surveyed before the construction of one the deep sea, smart quay walls in the Port of Rotterdam (Vos et. al 2015). Before back-filling the sea-bed level at the site was approximately -18 NAP (i.e. 18m below sea level). The geological conditions generally consist of a thin sand layer, underlain by clay and peat layers. Most engineering structures in the Port are supported in the very-strong Pleistocene sand layer that is evident at depths below -22 to -23.5m NAP across most of the section. In one area, the Clay layer (green) which has much lower strength and stiffness than the Pleistocene sand extends to a much deeper level, ≈ -32m. This represents an ancient river channel that cut through the sand deposit and has since been infilled by weak deltaic deposits. Any foundations installed in this layer would be expected to have much capacity and experience much larger displacements than those founded in the sand layer.

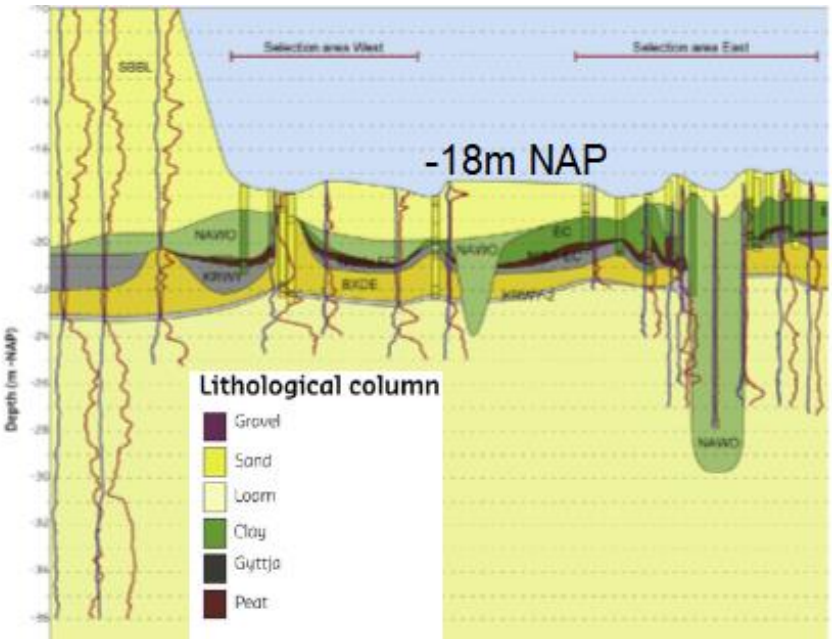

Figure 1 Pre-construction Geological Section at a smart quay wall location in the Port of Rotterdam (after Vos et al. 2015)

2.2 Soil-Structure interaction

During excavation the displacement of a retaining wall and the force generated in temporary of permanent supports such as struts or anchors are inter-linked, See Figure 2 . The first step in the analyses is to estimate the in-situ effective stress states that control the strength and stiffness and soil.

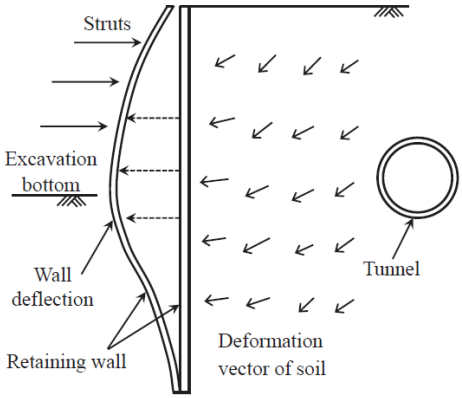

Figure 2 Soil structure interaction effects during excavation (Mu et al. 2023)

Whilst the in-situ vertical effective stress depends on the soil unit weight, the depth under consideration and the relative position of the water table. The horizontal effective stress is the most important property when calculating the force on a retaining wall. The horizontal and vertical effective stress are linked through the coefficient of earth pressure, K. Before construction of the retaining wall, the at-rest coefficient of earth pressure, K_0, which will vary with depth and with soil type and depends the geological history of the soil. As excavation progresses the K value changes as strain increases or decreases, See Figure 3. When the retaining wall moves towards the excavation, horizontal strains are negative and the force acting on the back wall reduces as K reduces towards a limiting minimum value, K_a. If the wall is pushing into the soils mass, the strain is positive and K increases towards a limiting value termed, K_p. This situation typically occurs near the bottom of a retaining wall, see Figure 2 where the wall is rotating.

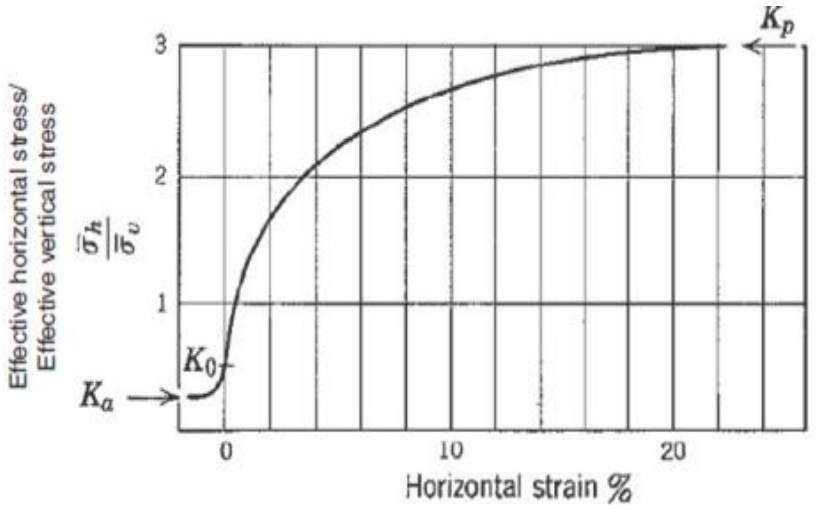

Figure 3 Effect of strain level on the coefficient of earth pressure

The strength of a soil depends on the mineralogy, stress level, geological history, loading rate and many other factors. One important aspect is the influence of the strain level, as shown in Figure 4a which plots the development of deviator stress, q with strain-level, ε in a laboratory element test on a soil sample. The data show the impact of stress level, σ'_3 (or soil depth) with the strength increasing significantly as the stress-level in the test increases. The highly non-linear response results in the soil stiffness (shear modulus, G) reducing with strain level, See Figure 4b.

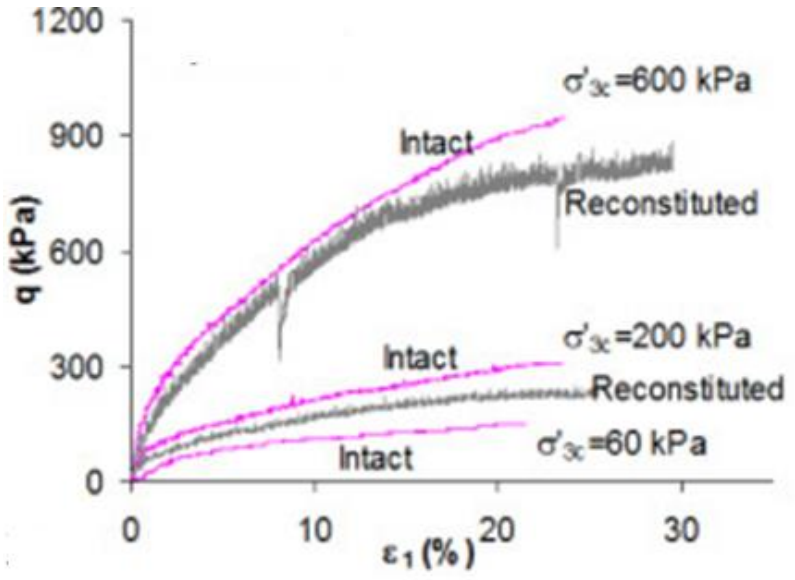

(a)

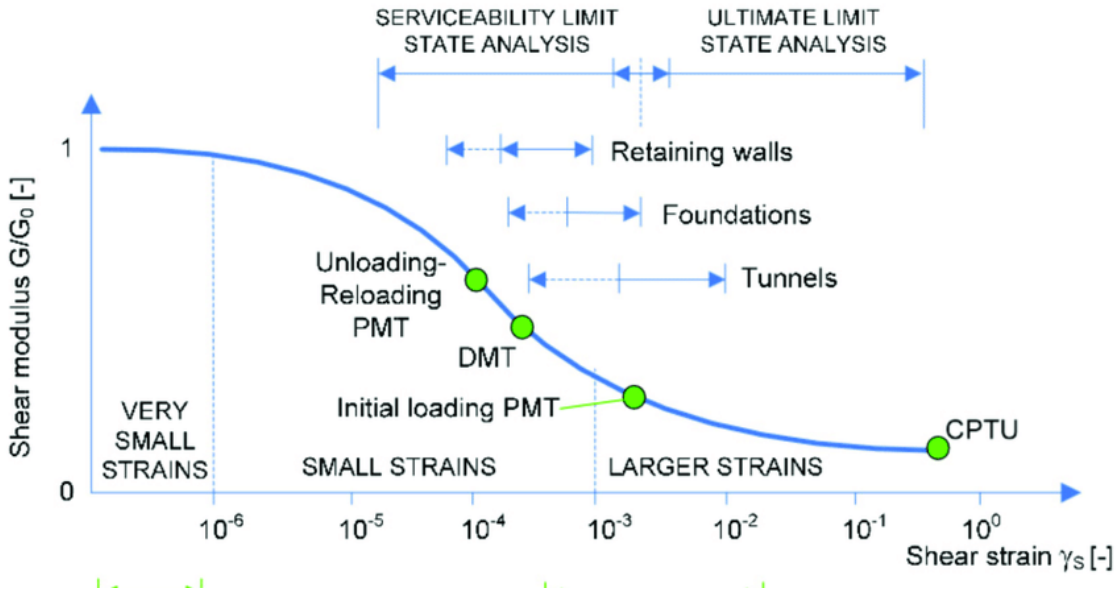

(b)

Figure 4 (a) Stress-Strain after Yi and Hitcher 2018 (b) Stiffness degradation response of a typical soil (after Popielski et al. 2022)

Predictions of the contours of horizontal displacement of soil behind a typical quay wall in the Port of Rotterdam are seen in Figure *5*. Large displacements (red shading) are concentrated immediately behind the wall, in a zone extending just below the bottom of the dredge level to approximately hallway up the dredged depth. This illustrates the range of strain states experienced even for a relatively simple structure.

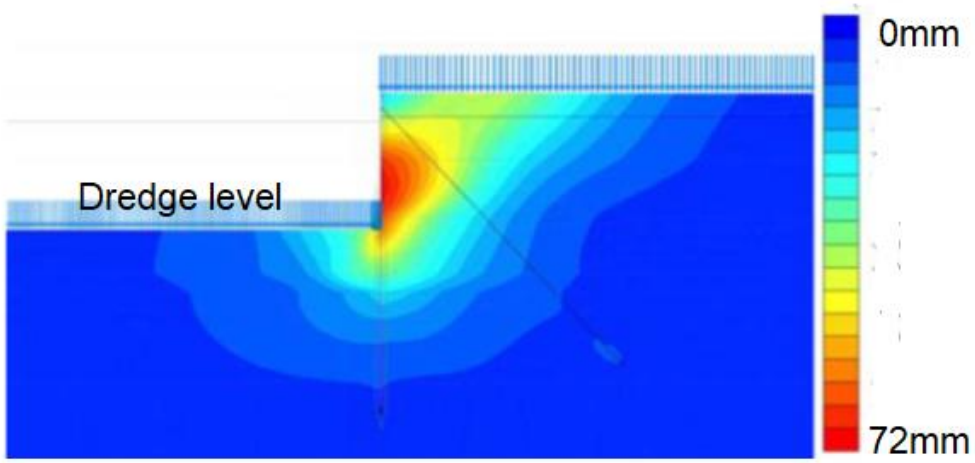

Figure 5 Distribution of horizontal displacement behind a quay wall in the Port of Rotterdam (Roubos et al. 2014)

2.3 Model Uncertainty

A deep-sea quay wall typically has a number of components, See Section 3, including geotechnical elements such as axially loaded piles and anchors. In design practice the geotechnical capacity of a pile or an anchor relies on two calculation models, one to estimate the shear resistance that develops along the pile shaft, chaft capacity. A second calculation is performed to estimate the vertical resistance at the pile base, base capacity. Because of the issues described in the preceding paragraphs, coupled with uncertainties about the impact of pile installation on the soil properties, calculation models to predict the capacity of piles and anchors are relatively unreliable, when compared to models for structural components for example. This uncertainty is illustrated from a prediction exercise published by Clayton (2000) where a number of respondents (A-P) predicted the failure load of a pile that was subsequently subjected to an axial load test to determine its resistance. The measured capacity (combining the shaft and base resistance) of the pile was approximately 2800 kN. The predictions can be seen to vary from a factor of 3 times too low (team A) to a factor of twice too high (team P).

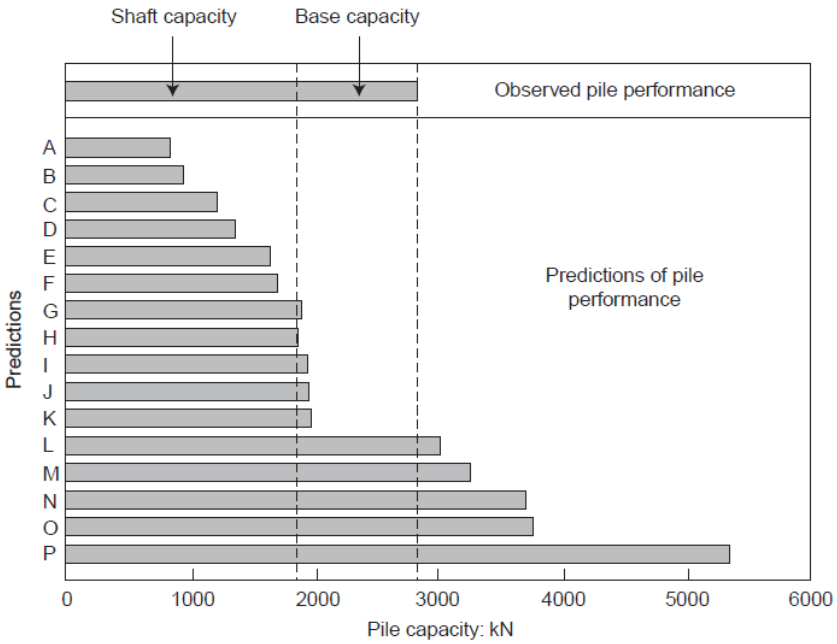

Figure 6 Comparison of measured and predicted pile capacities (Clayton 2000)

2.4 Examples of construction problems

Risks to construction include those associated with; (i) risk of harm to persons, (b) financial cost, (iii) delays to the timescale, (iv) damage of the environment and (v) impact on the quality of the finished construction. Given the natural variability of soil, complex construction processes in poor working environments and model uncertainty, failures are all too common. Endicott (2015) presents case studies of failed excavations listed in **Error! Reference source not found.**. The impact of such failures i s evident from Figure 7.

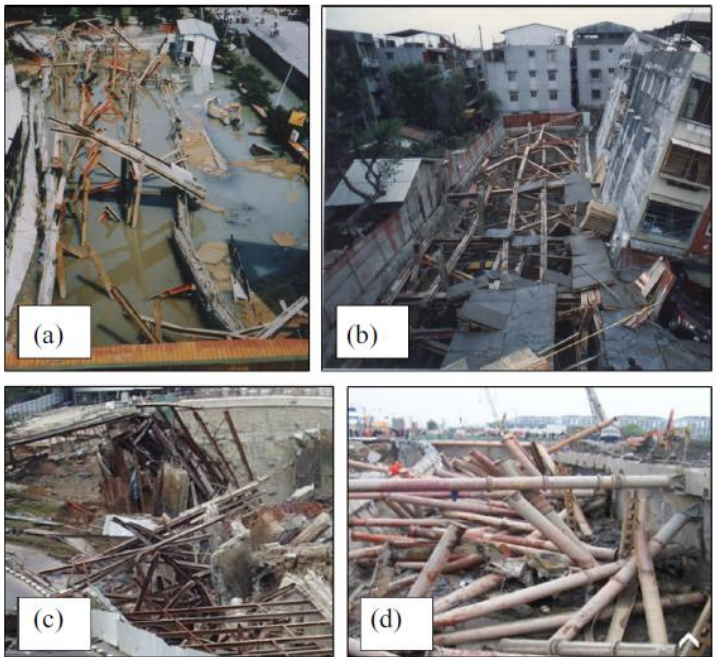

Figure 7 The impact of failure of urban excavations, Case (a) and (b) Taipei, (c) Nicoll Highway, Singapore and (d) Hangzhou, (from Do et al. (2016)

Location	Description of failure	Reason
Edinburgh Tower, Hong Kong (1981)	A two-level basements being constructed using temporary sheet piles failed when the base slab was under construction. Major impact on adjacent Queen's Road.	Rock levels were higher than predicted from the site investigation. Therefore, sheet pile toe levels were higher than expected, and when lower struts were removed for base slab construction failure occurred.
Taegu Metro Station, South Korea (2000)	A diaphragm wall was used to provide temporary support for the excavation of a cut and cover tunnel. An extensive collapse occurred which impacted the adjacent road in the busy urban setting.	The cause of failure was determined to be due to presence of high-permeability sad and clay layers that were not anticipated based on the site investigation.
Sao Paolo Metro (2007)	An access shaft for a tunnel boring machine, measuring 40m wide and 40m deep and a 45m long section of the adjacent station excavation collapsed.	The collapse was suspected to have been caused by fractured rock located above the station. Significant ground settlement of 20mm was recorded in the days before the failure.
Nicoll Highway, Singapore (2004)	A 33m deep excavation was being made to construct a tunnel using the cut and cover technique. Primary support was provided by diaphragm walls with internal steel struts. The excavation which was deeper than normal occurred before the 10th and final level of steel struts was installed.	A public enquiry found a number of reasons for the failure, including inconsistency between design criteria and codes, insufficient embedment of the wall, complex ground conditions and geometry.

Table 1 Cases of failure of deep excavations after Endicott (2015)

2.5 Digital twins applied to deep excavations

Geotechnical engineering projects face many uncertainties. To address natural variability we must perform a ground investigation to determine the stratigraphy and measure the soil properties at the location of the construction. Even for very high-value projects the percentage of the volume of the soil investigated is miniscule. Because of the impact of soil-structure interaction, installation and model uncertainty apriori prediction of geotechnical structures remains challenging. The observational method (Peck 1969), where monitoring is performed throughout the construction process allows modifications to the design is a powerful tool in dealing with these uncertainties.

Phoon et al. (2019) notes that the observational method is used to control risk at the construction stage, whilst factor of safety is used to control risk in the design phase. They note that unlike in other branches of civil engineering, e.g. structural engineering where design and construction are distinct, i.e. the column spacing in a building in not altered as floors are completed. In geotechnical engineering it is common for rock bolt spacings in tunnel excavation and strut or anchor spacing in an excavation to be adjusted depending on the observed response of some excavation stage. The UK Institution of Civil Engineers (ICE) State of the Nation Report (2017) highlights how advances in digital technology can allow advances in design that overcome some of the issue addressed in previous sections. Foremost was the ability to harness data on constructed in the management of said assets. Digital twins thus provide an excellent resource for implementing the observational method in projects in addition to providing other benefits, e.g. increased productivity (Gerbert et al. 2016).

Hong et al. (2022) developed a monitoring and management approach to manage risk during the construction of a subway station excavation pit in Shenzhen, China. Following the ground investigation the authors created a 3D geological model using BIM software (Revit 2020). The excavation was monitored using a range of sensors to monitor displacement, strain (See Figure 8) and a drone and machine vision was employed. The authors tested the ability of neural networks to predict settlements in the excavation pit. A digital twin comprising three functions, 3D visualisation, life-cycle monitoring and predictive analysis was proposed.

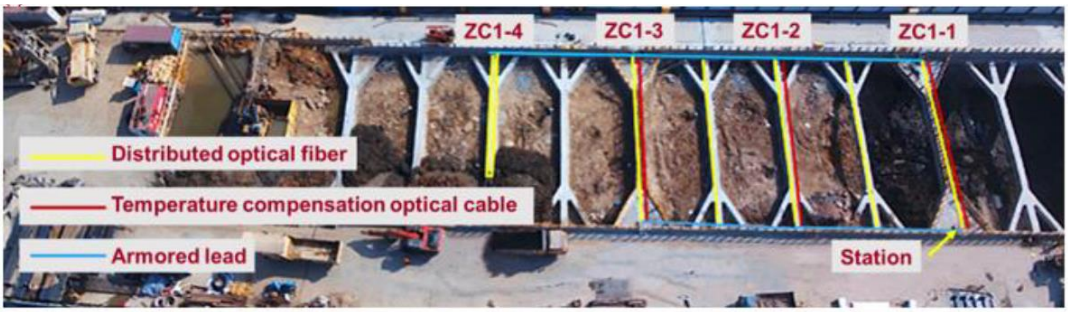

Figure 8 Monitoring of initial excavation in braced pit (Hong et al. 2022)

One of the major challenges facing projects where complex structures such as excavation pits are instrumented, is how to manage the vast streams of data collected. Fang et al. (2023) present a methodology for detection of anomalous readings and denoising such data and demonstrate their methodology on an excavation pit from the Wuhan metro project.

Sun et al. (2023) established a risk prediction and control method consisting of a digital twin of a deep excavation, See Figure 9. Methodology was applied to a real construction project, an excavation pit for the Wuhan metro line 7. The construction pit was supported by a retaining wall constructed using 1200 mm diameter contiguous bored piles with internal propping of concrete or steel beams at six levels of the

excavation. Vertical and horizontal displacements wall displacements were monitored throughout excavation and the data was used to update a finite element model of the wall. A warning system was established with a trigger-level displacement > 30mm. The soil was modelled using a simplified Mohr-Coulomb elastic-plastic model.

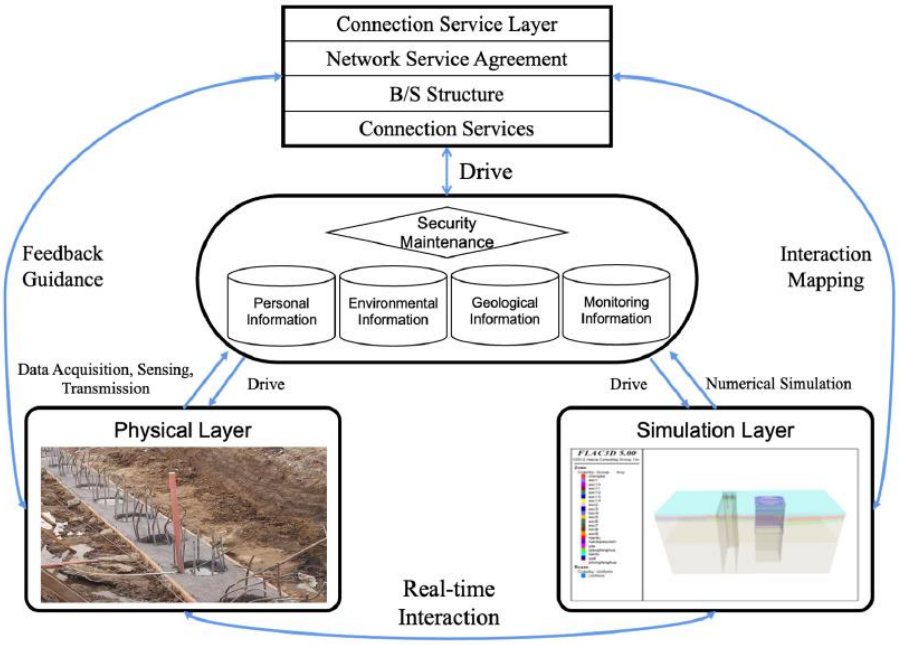

Figure 9 Digital Twin based prognosis and control framework (Sun et al. 2023)

2.6 Summary

In this section the risks involved in deep excavations and their impacts in projects were discussed. The sources of hazard were considered and a methodology, the observational method to control was these risks was identified. Digital twins provide a new opportunity to implement the observational method is a structured and controlled manner with full traceability of the processes. In the following sections of this report these opportunities are explored when applied to a deep sea wall construction using data from a Smart Quay wall constructed at the Port of Rotterdam.

3 BACKROUND TO DEMONSTRATION SITE

The Port of Rotterdam is one of the largest ports in the world. The port authority invests in sustainable and future proof design solutions with the aim to reduce the CO_2 emissions by 50% in 2030 and achieve a zero carbon footprint by 2050. One of the key steps in this process is optimising the design of all the components of port infrastructure. For the Port authority quay walls are the most important element of infrastructure. The Port is more than 600 years old and the authority manages many old quay walls and is currently constructing deep-sea quays in an area of land reclaimed from the North Sea known as Maasvlakte and Maasvlakte 2, indicated as the green and yellow areas in Figure 10. Because of the variable nature of the environment, scale and the complexity of the developments there are many uncertainties surrounding the evaluation of the current condition of existing assets and the design of new infrastructure. These include accurate estimation of their current safety level, their ability to resist additional loading and resilience to the impact of climate change. In recognising these challenges the port authority has been increasingly deploying sensors into its critical infrastructure assets in order to monitor their response in real-time. A number of Smart Quay walls have been heavily instrumented to measure the wall performance (wall displacement, load in various structural components) and external loading conditions, (crane loads, water level, temperature etc.) during operation.

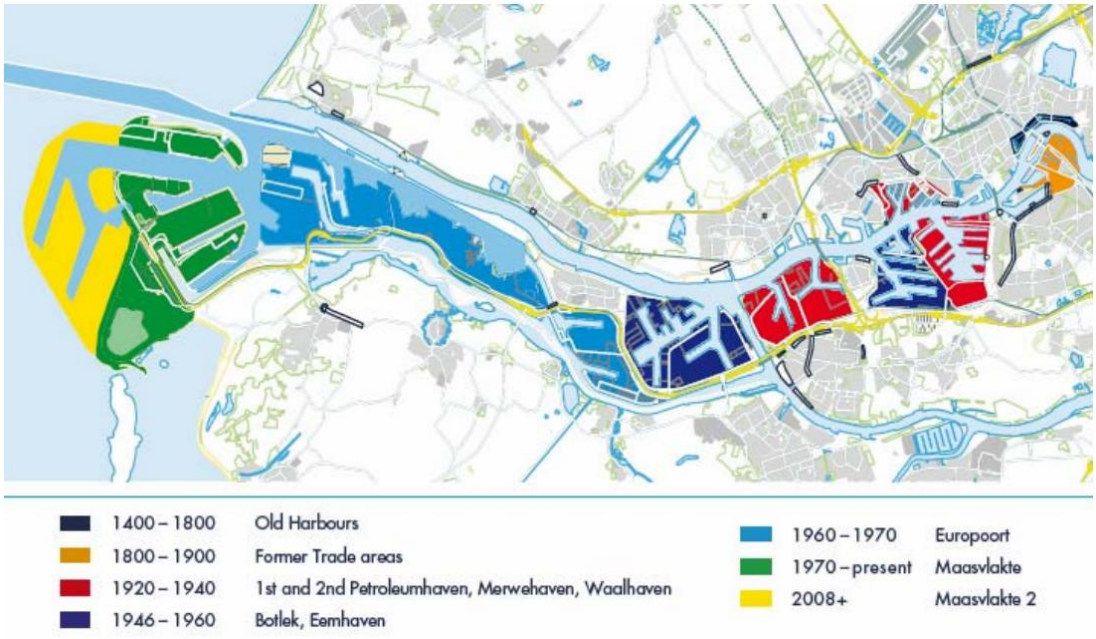

Figure 10 Areas of the port of Rotterdam. The quay wall considered in this report is located on the Maasvlakte in the west (de Gijt et al., 2010)

A quay wall is a complex system whose behaviour depends on a number of interacting components, See **Error! Reference source not found.**. The retaining wall that forms t he vertical restraint to the back-fill soil is usually formed with a flexible steel combined (combi)-wall form of construction. The advantage of flexible steel walls is that the deformation that occurs during dredging allows the backfill soil to move forward, thus reducing forces on the back of the wall. As the wall pushes into the soil on the seaward

side it efficiently mobilises the soil resistance below the dredge level thus providing lateral resistance against wall failure. Additional resistance is provided by steel tension anchors, driven deep into the soil on the landward side of the wall and connected to the relieving platform. During dredging the anchor force is mobilised as the wall tends to move outwards. The concrete relieving platform is a reinforced concrete structure placed atop the combi wall that is then backfilled with sand. It acts efficiently to reduce the effective span of the combi wall. The vertical loads from the relieving platform are transferred to deep soil layers by axially loaded steel or concrete pile foundations.

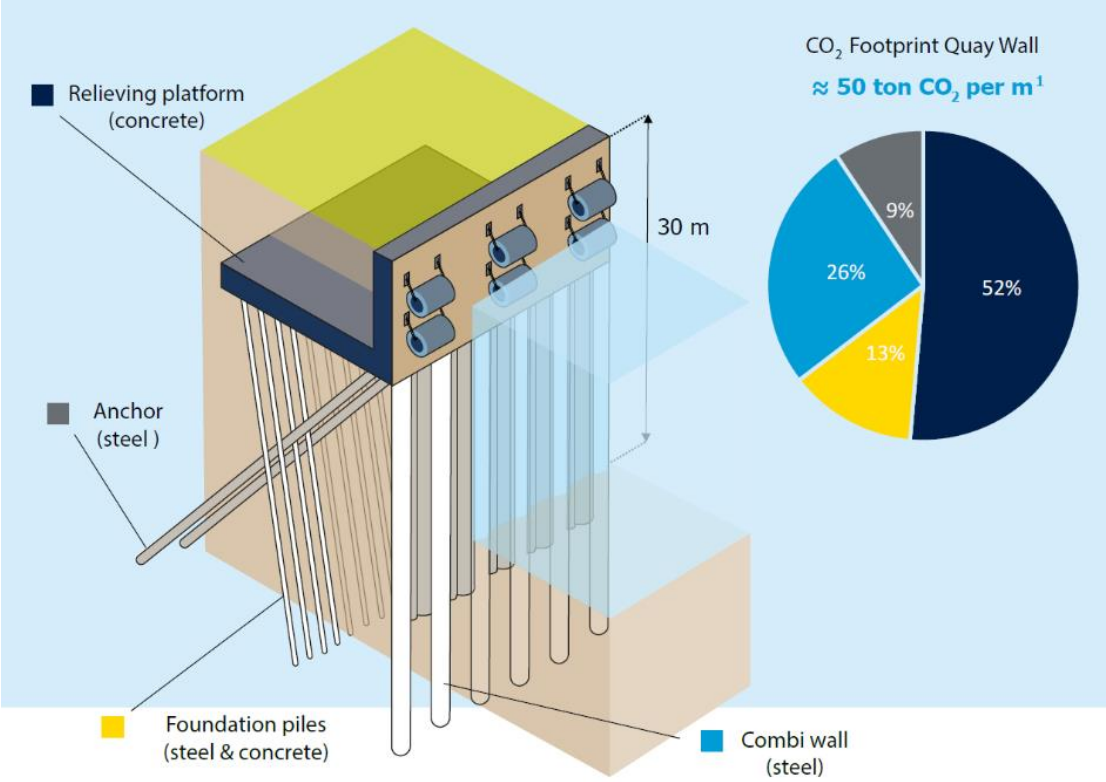

Figure 11 Components of a modern deep sea quay wall (Roubos 2019)

During the design of a new structure or assessment of an existing object an engineer must evaluate the resistance, R (capacity) available and compare this to the demand, D (loads applied). The structure is safe when the resistance, R exceeds the demand, D by an adequate safety margin. In traditional design a conservative estimate of the resistance is determined and this is compared to a low probability (or extreme) loading event.

There are a number of uncertainties associated with the approach:

(i) For the quay wall considered here, the retaining structure is embedded in highly variable soil and soil-structure interaction effects are dominant. Soil is a natural occurring variable material (unlike steel or concrete that are manufactured with controlled tolerances). This variability is particularly large in deltas with properties that vary over short distances both in the vertical and horizontal direction and are influenced by the response of the structure. For example the stresses or loads experienced in the combi wall are directly influenced by how much displacement occurs during construction and over the lifetime of the structure. When displacements are low (i.e. behind a more rigid wall) the load from the soil retained behind the back of the wall is

high and the resistance mobilised by the soil below the dredge level at the front of the wall is low. Thus a relatively flexible wall that allows movement to occur close to the displacement limit specified is much more efficient that a very stiff wall. The designer must consider a balancing act between limiting soil movements around the structure and allowing relaxation of the soil to reduce structural loads. As a result the choice of materials and the construction sequence can be designed to maximise the beneficial soil-structure interaction effects.

(ii) The capacity of all elements of the structure including the anchors and piles are determined using models. However, because of the complex stress and strain conditions induced by the combi wall, anchor and pile installation few analytical solutions are available and engineers rely on empirical (based on experience) methods. To handle uncertainties these empirical models tend to include a number of safety factors. Applying these models to new structure geometries and different soil conditions is likely to result in errors, with the potential to either underestimate or overestimate the resistance. Whilst a conservative estimate will result in inefficient design leading to unnecessary costs that could jeopardise the business case for a development, an un-conservative design is unsafe and could lead to failure.

(iii) The demand (load) and resistance (capacity) are not independent. The demand depends on different sources of external loading (e.g. from stored materials, traffic, vessel forces, water/waves etc.) many of which are temporal and will change over the lifetime of the object. For example storms can cause increased wave forces (demand) on quay walls, whilst coincident increased water content of soils due to rainfall infiltration reduces the strength and stiffness of the soil (resistance).

In order to address these uncertainties the port authority have a number of ongoing initiatives.

(i) The Smart Quay wall programme allows the actual response of a structure to be monitored and compared to model predictions.

(ii) Full-scale field test programmes have been undertaken to determine the actual resistance or capacity of various elements of the quay wall, including anchors, See Putteman et al. (2018), and the geotechnical capacity of a range of axially loaded pile foundations used to support the relieving platforms, See Duffy et al. (2022)

The focus of Deliverable 4.4 of the ASHVIN project is on soils related risks due to the construction of excavations. As a result this deliverable uses monitoring data collected from the construction of a deep sea quay wall to determine the real safety level of the wall throughout the construction programme and compare to predictions using an advanced finite element model. By comparing the measured and predicted response of the wall, a number of updates are initiated that incorporate the knowledge gathered and allow for reduction of uncertainty in a logical and consistent manner. Having established the current safety level, What-If scenarios are then implemented that allow the asset manager to consider maximising the utility of the asset.

4 DESCRIPTION OF CASE STUDY

4.1 Description of Quay Wall Components

The case considered is part of a new development in the Maasvlakte area that includes a 2200 metre long combi-wall form quay wall. The development site has a quay side ground level of +4.5m N.A.P with a deepest dredge level of -24.5m N.A.P considered herein giving a maximum retained soil height of 29m. A part of the quay wall is built without a relieving platform, however, the deepest section considered here includes a concrete relieving platform of the form shown in Figure 12.

Figure 12 Typical superstructure Broos paper on Brammen terminal (Broos 2010)

Screw-injection piles (SI) are used to transfer compressive axial load from the relieving platform. These piles are formed by twisting and pushing a steel casing into the ground. The SI has a sacrificial steel base plate at the end Figure *13*a, typically with a diameter larger than the steel casing. At the site in question the steel casing has a diameter of 609 mm and the tip diameter is 850 mm diameter. During installation grout is injected from the pile tip reducing the shaft resistance acting on the pile as it penetrates the ground. Once the pile reaches the desired penetration depth, the steel casing is filled with concrete. Over time both the concrete and external grout harden and the pile is assumed to have a constant cross-section of width 850mm, See Figure *13*b. The piles at this location were installed at a rake angle, See Figure 11 of between 9° and 16°.

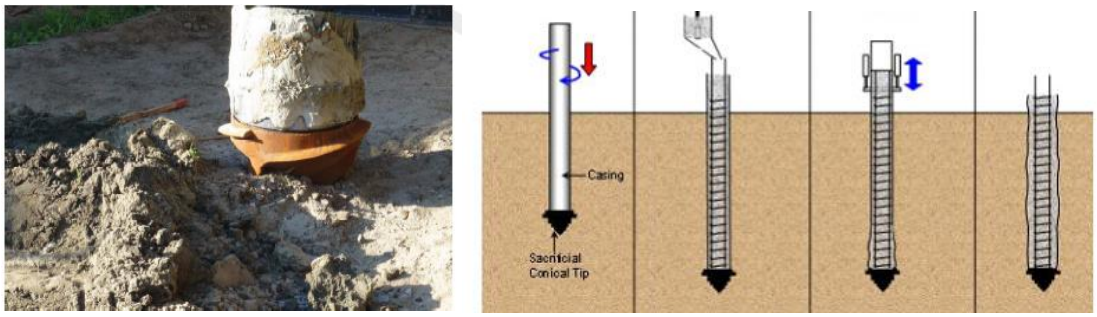

Figure 13 (a) Sacrificial end plate and (b) construction process showing final pile configuration (courtesy of Fundex Ltd.)

The combi wall is made-up of discrete 1420mm open-ended steel piles with continuity provided by interlocking PU 28 sheet piles. The open-ended piles are driven a number of metres into the deep Pleistocene sand layer, whilst the sheet piles are shorter, terminating just below the clay layer, See Figure 17.

Figure 14 Typical Combi Wall Construction
(https://constructalia.arcelormittal.com/en/products/combined_walls)

Lateral forces and bending moments in the combined wall are reduced through the use of Muller Verpress (MV) tension piles, See Figure 15a. These consist of a steel I-beam impact driven into the soil whilst injecting grout under pressure through two grout pipes mounted at the pile toe, See Figure 15b. During driving the fluid grout reduces shaft friction easing installation. After installation the hardened grout.

Figure 15 (a) Driving of an MV Pile (b) Pile toe showing grout tubes (Westerbeke 2021)

4.2 Construction Sequence

Construction of a deep sea quay wall involves many stages. In general a large fill area is first formed to provide a dry, safe working platform for construction operations, See Figure 16. After installation of the combi wall (Figure 14), construction of the relieving platform (Figure 12) and anchor installation (Figure 15) the seaward side of the quay wall is excavated (dredged) in stages.

Figure 16 Installation of large diameter open-ended piles for a deep sea quay wall (https://www.portofrotterdam.com/en/building-port/ongoing-projects)

The dredging stage is the time during construction when soil-structure interaction effects are most important. As the working platform and the soil on the seaward side of the quay wall is removed to form the shipping channel, displacement of the combi wall occurs. This mobilises movement of the retained soil and forces develop in the structural components (wall, piles and anchors). As noted the soil level on the landward

(quay) side of the wall is +4.5m N.A.P. The dredging sequence undertaken at the site is shown in Table 2.

Phase	Time	Dredge Level (m, N.A.P)
Dredging Stage 1	Day 1	-5.5
Dredging Stage 2	Day 9	-11
Dredging Stage 3	Day 12	-18
Dredging Stage 4	Day 51	-23
Dredging Stage 5	Day 74	-23 (berm removed)
Dredging Stage 6	Day 104	-24.5

Table 2 Dredging Sequence for the Quay Wall

A cross-section through the combi wall showing the soil layering and the final excavation level of -24.5m N.A.P is shown in Figure 17 below.

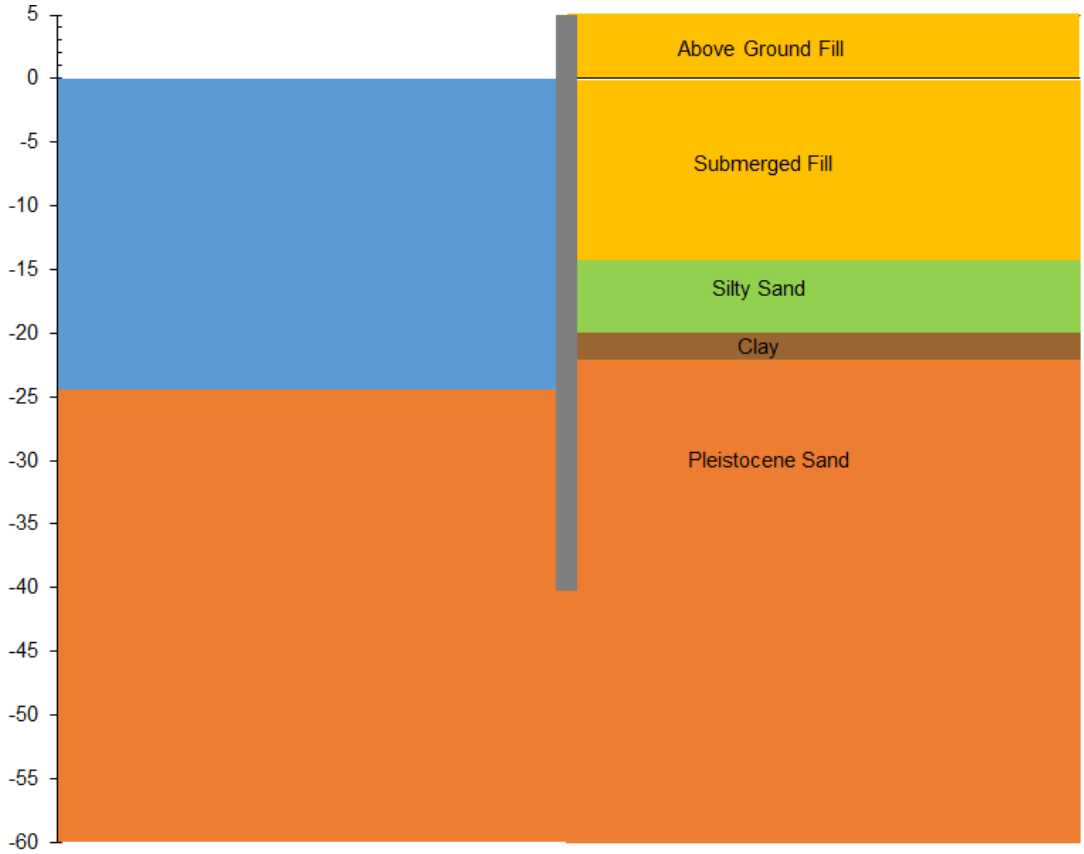

Figure 17 Final dredge level in front of Combi Wall

5 SOIL CONDITIONS

5.1 Introduction

The quay wall is located in the Maasvlakte area of Rotterdam Harbour. The Maasvlakte, lies in a Delta region of the Rhine-Meuse. Large-scale sand reclamation which formed the Maasvlakte began in the region around 50 years ago. Delta regions are usually areas where near surface soft soils exist. At the Massvlakte, the original surface deposits have been affected by geological process and then buried beneath a deep fill predominantly sand, fill layer.

5.2 Ground Investigation

An extensive site investigation consisted primarily of Cone Penetration Testing, CPTs supplemented by boreholes and laboratory testing. During a CPT test, a cone of standard dimensions, See Figure 18 is penetrated into the ground at a constant rate. A number of useful quantities are measured continuously during cone penetration, these include, the vertical stress at the cone tip, q_c and the sleeve friction f_s. Other parameters can also be measured, such as the pore water pressure, u_2, and the shear wave modulus, v_s. One of the earliest applications of CPT data was as a soil profiling tool. The friction ratio, $F_r = f_s/q_c$ %, is a powerful method of classifying soils (identifying soil type) with sands typically having friction ratios of around 1% with F_r increasing as the soil becomes finer with clay typically having F_r in the range 3 to 5%.

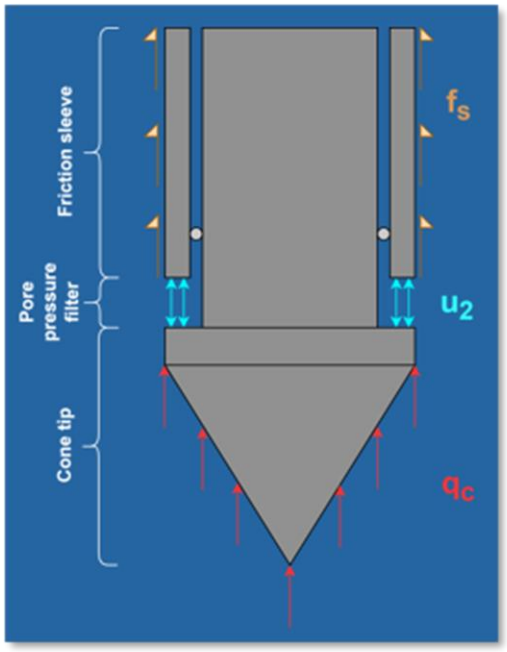

Figure 18 Components of a CPT cone and definition of parameters measured

The original sea bed level (before land reclamation) at the site was -14m N.A.P. Prior to construction of the quay wall, the ground level at the site was close to mean sea level ≈0m N.A.P, which corresponds to the mean average water table level at the site. CPT data acquired during the site investigation are shown in Figure 19 reveal:

- A fill layer from ground level to approximately 14m below ground level is predominantly sand, $F_r \approx 1\%$ with a q_c value in the range 10 to 30 MPa. The fill

material was dredged from the North Sea and inland lakes and appears to contain occasionally weaker clay lenses (low q_c and F_r of 3 to 5%).

- Below the fill layer there is an estuarine deposit, known as the Naaldwijk formation. This layer is present from -14m to -20 N.A.P. The CPT q_c values reduce with depth in this later whilst the F_r values increase. This is indicative of a more sandy deposit fining with depth to become clay rich.
- At ≈-20m N.A.P (the top of this layer can vary by ±1m) there a is a 2-3m thick layer of Wijchen Clay. The q_c value of this layer is generally in the range 1 to 3 MPa.
- Below is the Pleistocene sand layer the top of which is generally around -22 to -24 m N.A.P. CPT q_c values in the area typically range from 15 MPa to 60 MPa. However, thin clay lenses, generally less than 1m thick, with qc values similar to the Wijchen Clay are commonly found in this deposit. Evidence of these clay lenses are indicated by the CPT profiles in Figure *19* with low q_c and high F_r values at -27m and -37m N.A.P.

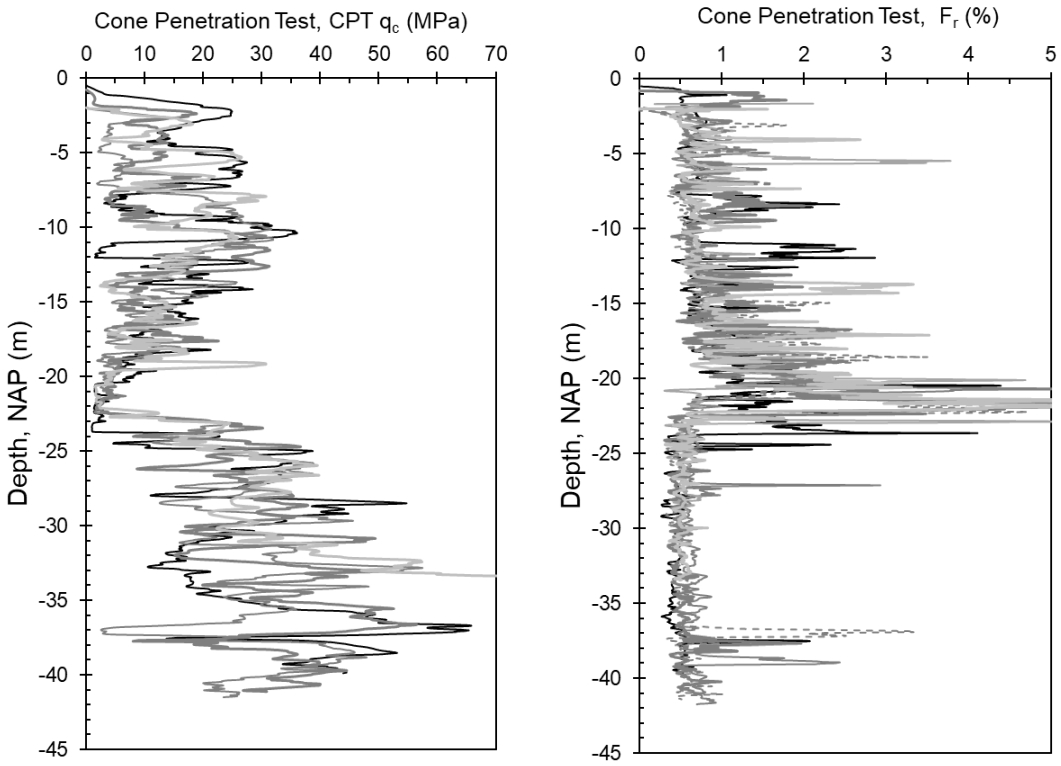

Figure 19 CPT data measured prior to Quay Wall Construction
(a) CPT q_c with depth, (b) F_r with depth

5.3 Soil variability

Given the quay wall is a long, linear structure, in this report a section with the heaviest concentration of instrumentation that provided high-quality data throughout the construction process was selected for analysis. In this analyses the CPT q_c value is used extensively to derive representative soil properties or directly to determine pile or anchor resistance. Soil is a naturally occurring material with depositional variability, is anisotropic with variability in both the vertical and horizontal direction in addition to having properties that vary with stress and strain-level. It is important to capture this soil variability in design. One of the advantages of using CPT q_c values is that they

capture this variability, given large volumes of measurements with which to consider point statistics. An important point when trying to quantify variability is to consider the volume of soil affected by the geotechnical structure. In Figure 20 the relatively small displacement field (volume of soil) affected by axial loading a pile to failure is compared to the large displacement field around an embedded retaining wall as excavation reaches its final level. It is apparent that:

- The base resistance of the concrete pile (pile is shaded orange in Figure 20a) develops in a soil volume concentrated 2.5 pile diameters below, 2 pile diameters above and one diameter each side of the pile. Given the typical diameter of such a pile is less than 0.5m the volume of soil affected is small.
- In contrast, See Figure 20b the width of the active (behind) and passive zones (in front) of the retaining wall where soil displacements occur are approximately equal to the excavation depth. As a result a very large volume of soil is mobilised.

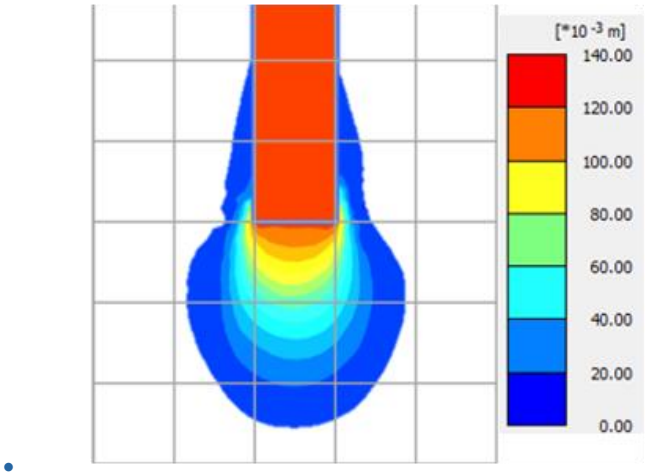

(a)

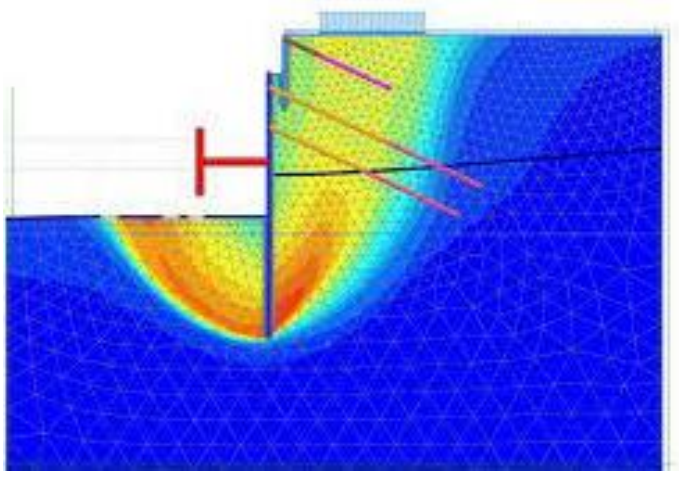

(b)

- Figure 20 Displacement field (a) around the base of a pile (Chai et al. 2023) and (b) around an embedded wall (https://www.geotech.hr/en/prop-loads-in-embedded-retaining-structures/)

A large number of CPT profiles in the area around the instrumented section were collated and the three CPT traces closest to the wall are compared to the mean from all CPT traces in Figure 21.

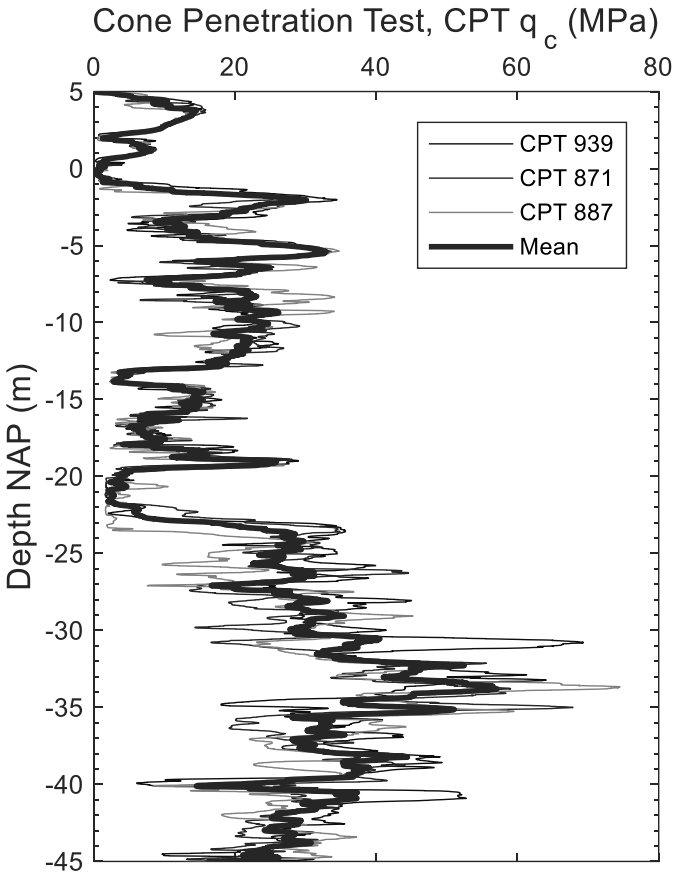

Figure 21 CPT traces closest to instrumented wall section

The CPT data after filling to the final construction level, +4.5m was statistically analysed to investigate each geological layer for any stratification, e.g. the presence of sub-layering or depth trends etc. For example considering the fill layer extending from 0m N.A.P to -14m N.A.P, the material is man-made from sandy soil and soil the soil behaviour could thus be assumed as reasonably consistent with depth as a result.

However, there is considerably dispersal in the strength behaviour with tip resistance varying from high to low values over regular (approximately 4m intervals), See Figure 21. We can also see in Figure 19b sharp sudden spikes in the friction ratio accompanying these drops in tip resistance again signalling the presence of thin weaker clay or silt layers. This behaviour is likely due to the sand blowing construction method employed to make the layers which are placed below water level (submerged), where sandy soil was sprayed underneath a ship to form new layers, dropping several metres of soil at a time. This would have caused lighter particles such as silts and clays to become suspended within the water and slowly flocculate down to the seafloor resulting in the development of regular sediment layers of similar particle size. While this layer has significant variation within it and exhibits a wide range of soil behaviour it was considered appropriate to treat it as a single layer within the analysis as the material was evenly distributed between areas of high and low strength with a

consistent scale of fluctuation, which ultimately would allow for the strength values to average out over the layer. Figure 22 shows a histogram of the q_c values in the layer with a normal distribution fitted, showing an extremely good fit achieved outside of the distribution tails .

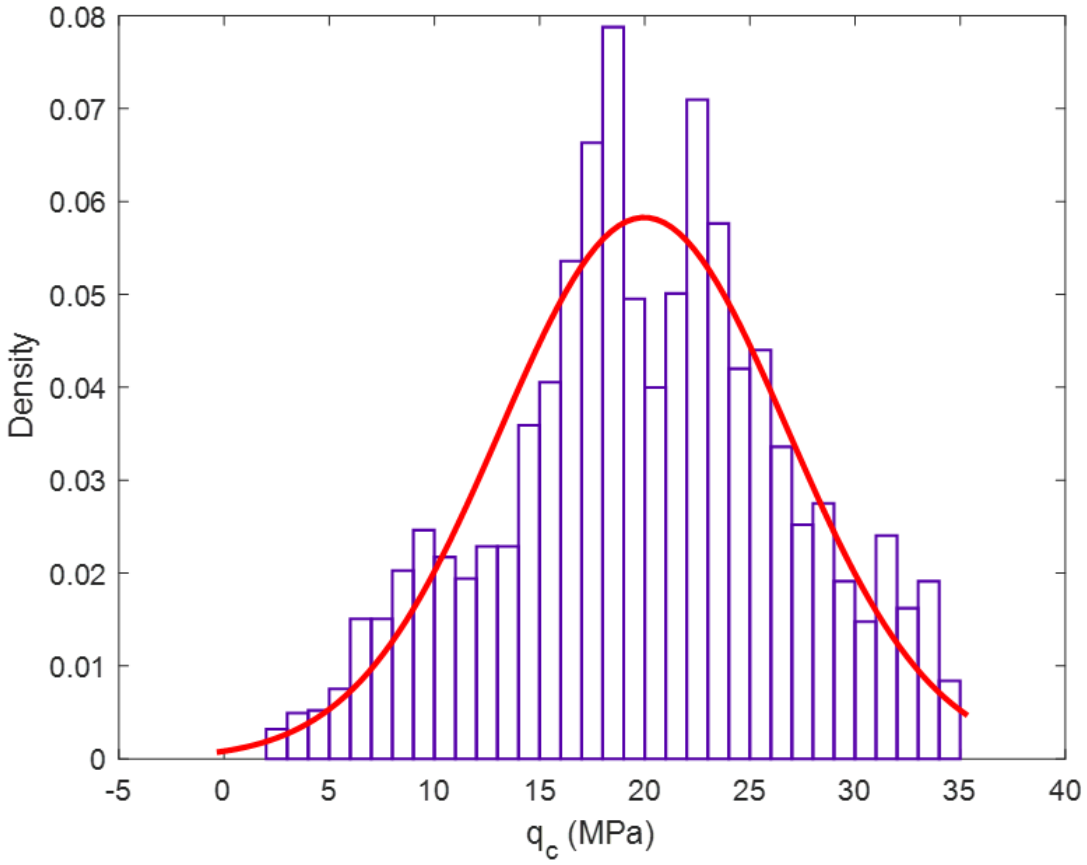

Figure 22 Distribution of q_c in the submerged fill layer with a normal distribution fitted

From the perspective of the geotechnical capacity of the piles, anchors and the passive resistance of the quay wall, the most important soil bearing layer is the Pleistocene sand layer below -22m N.A.P. Any trend for the strength to vary with depth or for the occasional clay lenses to interfere with the mass properties should be accounted for in the design. The point statistics for the Pleistocene sand layer, See Figure 23 reveal a lognormal fit shows very good agreement, except for the LHS tail (low q_c range) where data from the intermittent clay lenses skews the histogram. The red line considers all data, blue excludes the clay. There is no significant difference in means between the two distributions, however the red distribution has a slightly larger standard deviation.

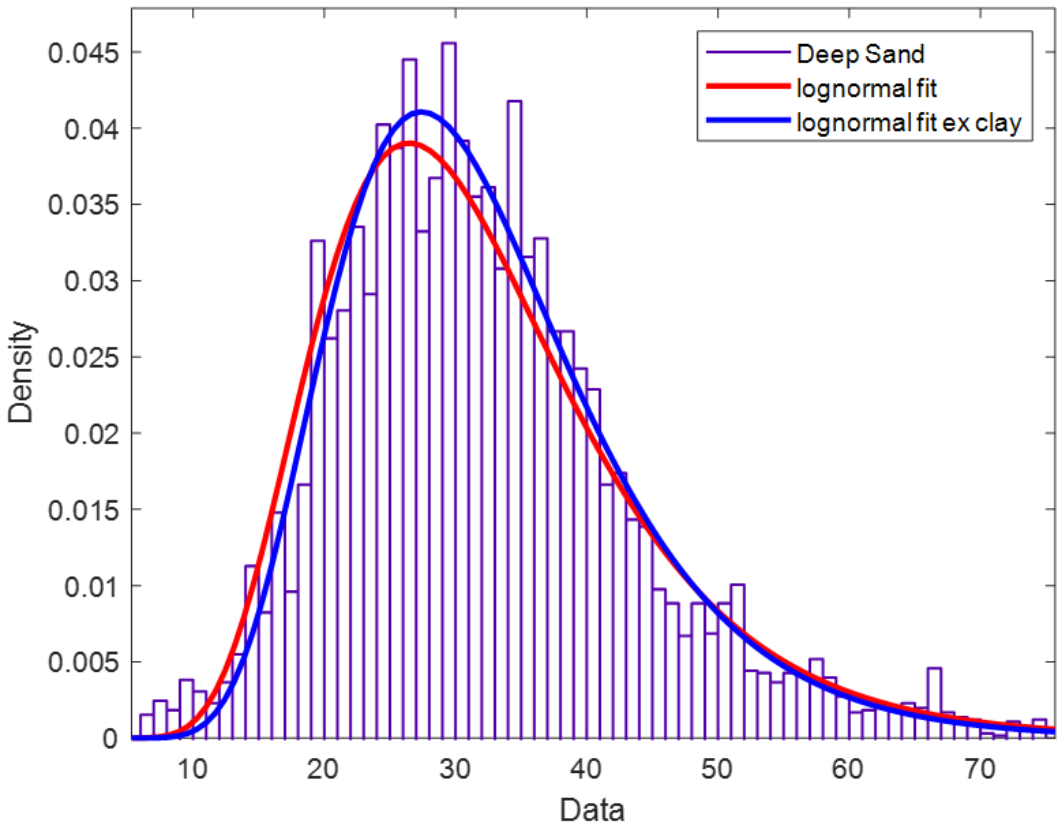

Figure 23 Point statistics in the deep Pleistocene sand layer

Similar analyses for all the soil layers allowed the soil profile to be simplified into 5 layers, See Figure 24 described by the mean strength q_c values and with no sub-layering or depth trends. The key CPT data is summarised for each layer in Table *3*.

Layer	Description	Depth (N.A.P) m	q_c (kPa)	Q_{tn}	I_c
1	Above Ground Fill	+5 to 0	7,200	159	1.66
2	Submerged Fill	0 to -14	20,200	137	1.68
3	Silty Sand	-14 to -20	11,200	48	1.81
4	Clay	-20 to -22	1,700	-	
5	Pleistocene Sand	-22 to -40	32,100	109	1.71

Table 3 CPT q_c values for each soil layer

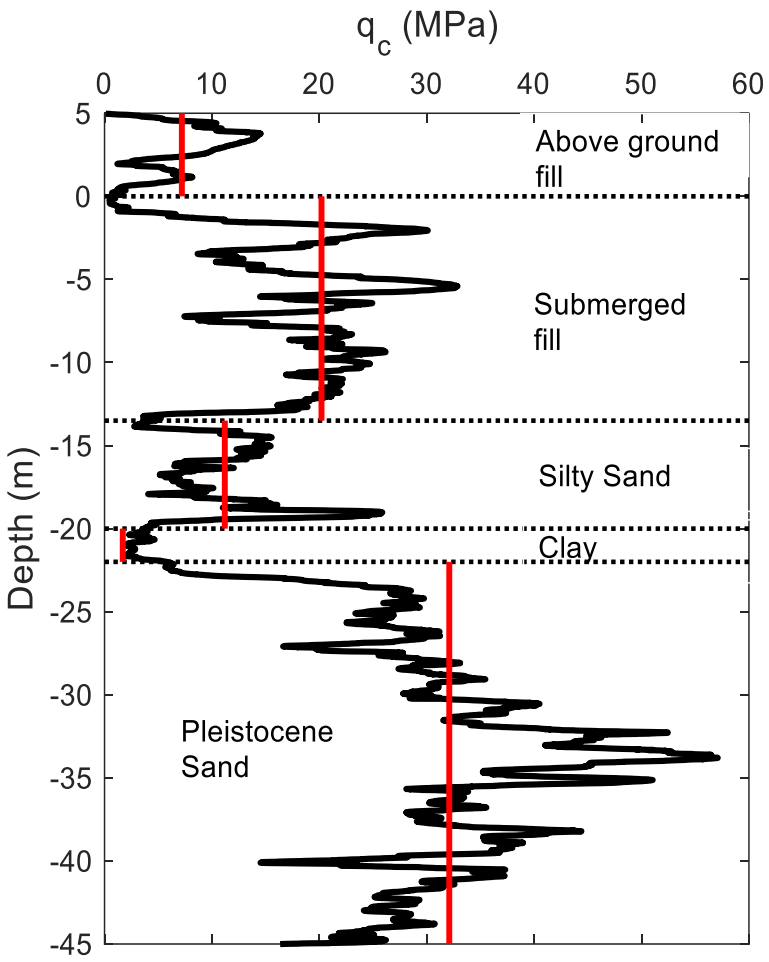

Figure 24 Simplified Soil profile adopted for the key wall analysis

Given that the cone resistance is dependent on the mechanical behaviour of soil, e.g. strength, stiffness compressibility and drainage Robertson (1990) suggested that the charts were predictive of soil behaviour type, SBT (i.e. they give information on how the soil responds to loading). This led to the development of soil behaviour type index, I_c which defines boundaries between behaviour types, See Figure 25.

$$I_c = \sqrt{(3.47 - \log Q_{tn})^2 + (\log F_r + 1.22)^2}$$ Equation 1

and

$$Q_{tn} = \left(\frac{q_t - \sigma_v}{P_{atm}}\right)\left(\frac{P_{atm}}{\sigma'_v}\right)^n$$ Equation 2

Where: $q_t = q_c$ in sand, σ_{vo} and σ'_{vo} is the total and effective vertical stress and P_{atm}= 100 kPa.

The layers 1,2,3 and 5 in our model plot in the sand behaviour range and a number of workers have proposed correlations between q_c and soil properties that are useful for modelling. These are described in the following section.

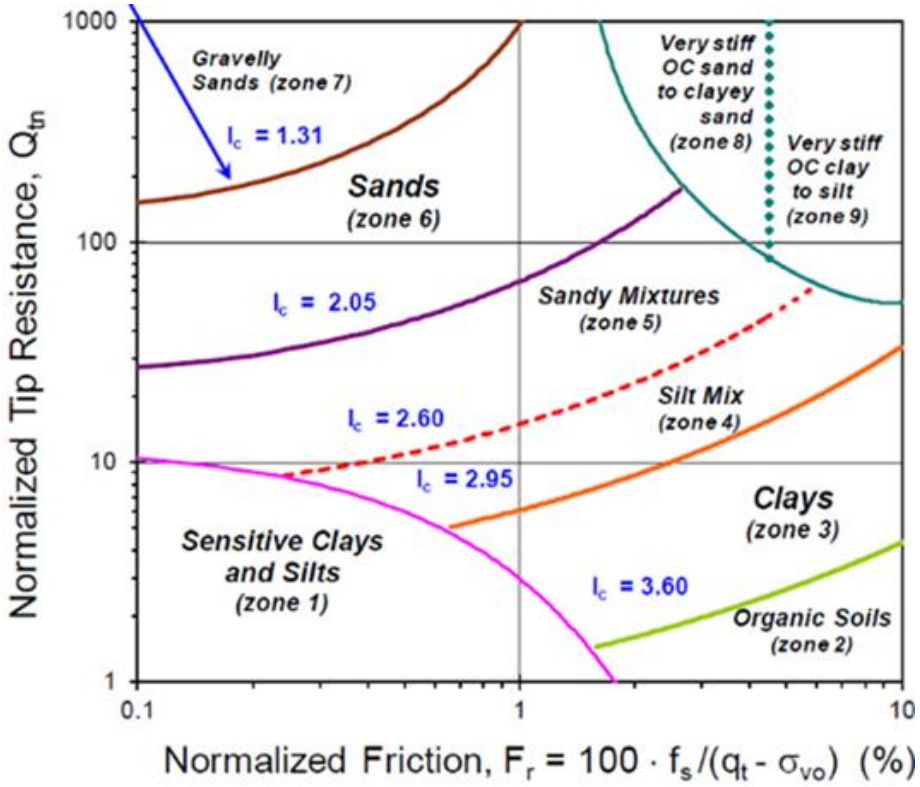

Figure 25 Soil behaviour type and soil behaviour type index

6 MODELING

6.1 Soil Properties

As quay walls are long-linear structures with relatively uniform form stretch for 100's of metres, modelling in plane-strain (2D) conditions is valid and efficient. The modelling work described in the following was performed using Plaxis 2D. The model allows the construction excavation sequence described in Table 2 to be modelled explicitly. Plaxis is a specialist geotechnical engineering tool and as a result has many advanced soil models that can be employed in analysis. The analysis of the quay wall undertaken firstly using the Hardening Soil model (HS), described by Schanz et al. (1999) and subsequently using the Hardening Soil Small-strain (HSS) model which accounts for high-stiffness evident in soils at small strains. The parameters required for the HS and HSS soil models are outline in Table 4.

Parameter Definition	Details
Unit Weight, γ (kPa)	$\gamma/\gamma_w = 1.22 + 0.15 \cdot \ln(100 * f_s/P_{atm} + 0.01)$ Where γ_w is the unit weight of water
Past maximum vertical effective stress, σ'_p	$\sigma'_p = 0.32\ q_c^{0.7}$
Over Consolidation Ratio, OCR	$OCR = \sigma'_p / \sigma'_v$
Peak friction angle, ϕ'_p	$\phi'_p\ ° = 17.6 + 11 \log Q_{tn}$
Lateral earth pressure coefficient at rest, K_0	$K_0 = (1-\sin\phi'_p)\quad OCR^{\sin\phi'_p}$
Density , D_r	$D_r = \frac{1}{2.91}\ln\left(\frac{\lambda\, q_c}{60\ \sigma'_v{}^{0.7}}\right)$ If the sand is a normally consolidated recent deposit, λ = 1, if an aged, over-consolidated deposit, λ = 2/3.
Reference secant stiffness in standard drained triaxial test, $E_{50,ref}$	$E_{50,ref} = E_{oed,ref}$ - Sand $E_{50,ref} = 1.25\ E_{oed,ref}$ - Clay
Reference tangent stiffness for primary oedometer loading, $E_{oed,ref}$	$E_{oed} = 5q_c$
Reference unloading/reloading stiffness, $E_{ur,ref}$	$E_{ur,ref} = 3\ E_{oed}$ – Sand $E_{ur,ref} = 5\ E_{oed}$ – Clay
Reference shear modulus at very small strains, $G_{0,ref}$	Measured in Geophysical Survey
Power for the stress-level dependency of stiffness, m	$M = 0.7 - (D_r/320)$
Shear strain at which $G_{sec} = 0.7G_0$	$\gamma_{0.7} = \frac{0.385}{4G_0}\left[2c\left(1+\cos 2\phi'_p\right) + \sigma'_{v0}\left(1+K_0\right)\sin 2\phi'_p\right]$

Table 4 Determination of Soil Properties

6.2 Pile Properties

The properties of the piles consist of structural properties, e.g. the stiffness and geometry of steel and concrete components and the geotechnical resistance. As the report is concerned with geotechnical uncertainty, the specified geometry and structural properties of the foundation elements (SI and MV piles) are assumed constant throughout the analyses. The geotechnical resistance of the piles were initially based on standard code procedures in Model 1. Thereafter, updated soil resistances determined from recent full-scale load tests performed at the construction site (MV piles) and a nearby construction project (SI Piles) are used to update the pile resistance.

6.2.1 Structural Properties

The geometry and structural properties inputted to model are shown in Table

Element	Dimensions (mm)	Spacing (mm)	E (kN/m^2)	A (mm^2)	EI (mm^4/m)
Open-Ended Steel Tube	D = 1420 mm t = 24mm	3295	210×10^6	40672	1.557×10^6
Sheet Pile	W = 1800 H = 454	3295	210×10^6	120	1.622×10^6
SI Pile	D_s = 609 D_b = 850	3295	210×10^6 30×10^6	Steel 5715 Con 82715	256×10^6 1794×10^6
MV Pile	H = 600 W = 300	3295	210×10^6	8195	520×10^6
Relieving Platform	Floor 16800x1750 Wall 2800x7000	-	30×10^6	175×10^4 280×10^4	44615×10^6 1829000×10^6

Table 5 Structural Properties

(Note: D, pile diameter, t, wall thickness, W, width, H, Height, D_s, shaft diameter, D_b, base diameter)

6.2.2 Geotechnical Properties – SI Piles

The axial capacity of a compression piles is comprised of two components, friction developed along the pile shaft, τ_f and end bearing resistance at the pile tip, q_b. In the current Dutch code, a CPT based design method links the shaft and base resistance components directly to the cone end resistance, q_c measured during the CPT test using constant reduction factors α_s and α_p to calculate the unit shaft, τ_f and base resistance, q_b respectively:

$$\tau_f = \alpha_s \, q_c \qquad \text{Equation 3}$$

$$q_b = \alpha_p \, q_c \qquad \text{Equation 4}$$

For the SI piles used in the quay wall, α_s = 0.009 and α_p = 0.63. The CPT q_c value used in Equation 3 is limited to maximum value between 12 MPa and 15 MPa, depending on the thickness of the bearing layers. The lower CPT q_c value is used when

the layer considered is less than 1 m thick. For the calculation of base resistance the q_c value is evaluated using the Koppejan technique wherein q_c is evaluated over a zone of 0.7 to 4D below the pile tip and 8D above the pile tip, where D is the pile diameter. The derived unit base resistance is limited to a maximum value of 15 MPa. The code requires use of the rules unless full-scale load tests are performed on at least three piles of comparable geometry in the soil conditions considered.

Duffy et al. (2022) described a load test programme performed on four SI piles in the Port of Rotterdam. The pile tests were carried out to optimise the design of piles for a new quay wall development. The ground conditions at the site are shown in Figure 26 to be comparable to the site considered in this report. The fill sand layer extends to -14m N.A.P, the silty sand layer extends to -24m N.A.P. This is underlain by a 2m thick clay. The Pleistocene sand has CPT q_c values in the range 30 to 80 MPa.

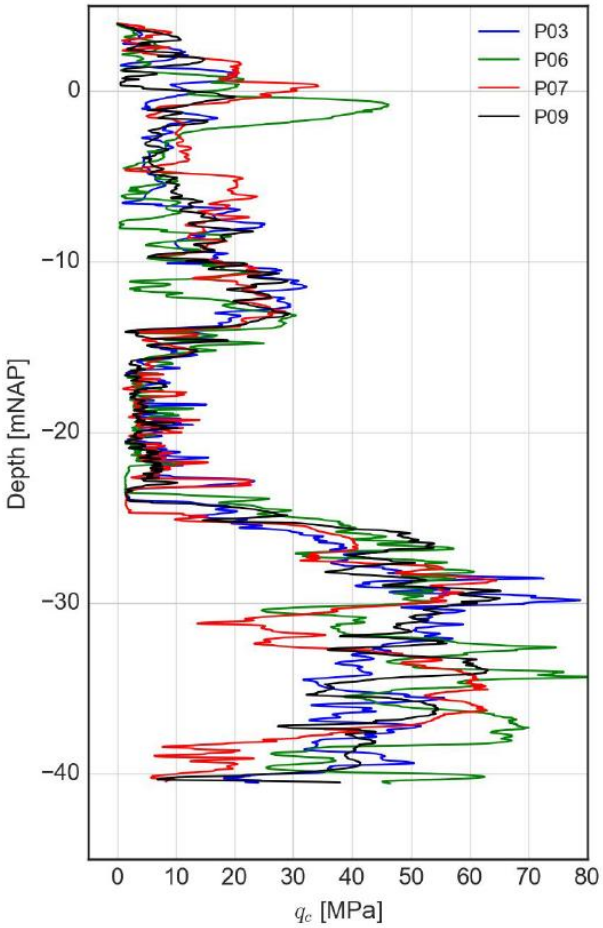

Figure 26 Ground conditions at the location of SI test piles

The SI piles had a screw tip diameter of 850 mm, outer tube diameter of 610 mm and tube thickness of 24 mm. Two of piles, P04 and P05, were installed to a depth of 37m below ground level, whilst piles P06 and P07 were ≈35m long. The variable soil lengths were chosen to investigate regions of higher and lower q_c at the pile tip.

The SI piles were installed through a combination of pulldown force and torque, whilst a grout mixture was injected horizontally from the pile tip, passing along the side of the pile and back up to the surface. The steel tube was filled with concrete after installation.

The piles were load tested in compression between 43 days and 95 days after installation. Compression load tests were applied in (typically eight) increments until a maximum load resistance was measured or the pile base settled by more than 10% of the pile diameter. To distinguish between the base and shaft resistances of the piles, deformation along the full-length of the pile was measured during load testing using two different fibre optic measurement systems: Fibre Bragg Grating (FBG) and Brillouin Optical Frequency Domain Analysis (BOFDA).

The shorter piles developed a peak capacity of between 16 and 17 MN. Although only 2m longer, the 37m long piles had their tips embedded in sand with significantly higher q_c value and developed maximum test loads of between 21.5 and 23.5 MN. The fiber optic strain gauges allowed the load-distribution down the pile and the ultimate unit shaft and base resistance of the piles to be determined.

The peak shaft resistance mobilised in the load tests on four piles is plotted against the normalised pile depth in Figure 27. The distance from the pile tip, h is normalised by the pile diameter D in the figure, therefore h/D = 0 is the pile tip, whilst 45 is ground level. What is noticeable is that the distribution of shaft resistance in Figure 27 closely mirrors the CPT q_c values in Figure 26 suggesting a direct correlation between τ_f and q_c as inferred by Equation 3. The measured shear stress profiles (discrete points) are compared with predictions of shear stress made using the current Dutch code, α_s = 0.009 and q_c limited to 15 MPa, dashed line in Figure 27. It is apparent that the approach gives reasonable estimate of the shaft resistance in layers where the CPT

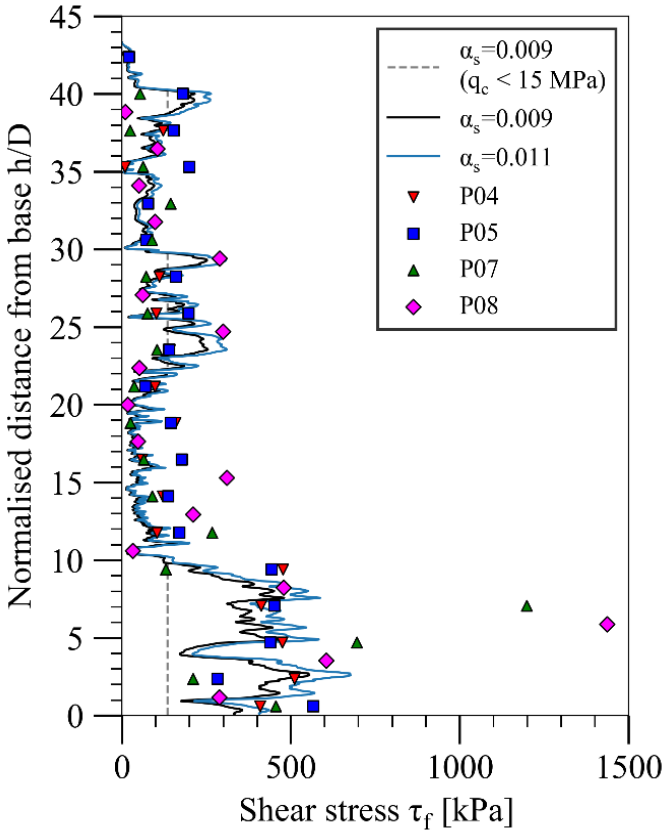

Figure 27 Ultimate shaft resistance mobilised in load test against distance from the pile tip (h/D)

resistance is lower than 15 MPa. However, in the Pleistocene sand layer near the pile tip (h/D values between 0 and 10) the shaft resistance is grossly under-estimated. Removing the limiting q_c value and applying the code value of α_s = 0.009 to the actual CPT q_c value measured (black line) results in a much better approximation of the measured shaft resistance. Duffy et al. (2022) suggest an α_s value of 0.011 with no limit on q_c (cyan line) gives a reliable prediction of the shaft resistance of SI piles. Whilst the shaft resistance of SI piles was much higher than predicted using the code approach in contrast the base resistance was much lower than predicted. The base resistance was similar to values measured for bored piles in sand, Gavin et al. (2013). As a result the following equations are suggested for the design of SI piles which were adopted in the design described herein:

$$\tau_f = 0.011\ q_c \qquad \text{Equation 5}$$

$$q_b = 0.2\ q_c \qquad \text{Equation 6}$$

6.2.3 Geotechnical Properties – MV Piles

Design practice in the Netherlands uses CPT based reduction factors to determine tension shaft resistance of anchor piles such as MV Piles.

$$q_{st} = \alpha_t\ q_c \qquad \text{Equation 7}$$

For tension anchors the reduction factor, α_t is 0.015 (CUR 166). The code also includes a national limiting maximum CPT q_c value for use in Equation 1, in the range 12-15 MPa that is dependent on soil layering. Based on previous load testing in the Port (de Gigt and Brassinga 1990) a higher limit value of 18 MPa is allowed in the Massvlakte area. Thus the limiting maximum shaft resistance of MV piles in the area is 252 kPa.

Six load tests were performed on MV piles installed at the quay wall project modelled in this report. The MV were load tested in tension using the load frame shown in Figure 28.

Figure 28 Load frame used for MV Pile tests

The load tests were performed up to geotechnical failure with the piles being instrumented along their full length with fiber optic strain gauges. This allowed the distribution of shaft resistance with depth to be determined. The distribution of load in

with depth in a pile, as the applied load increased from 2100 to 9541 kN is shown in Figure 29.

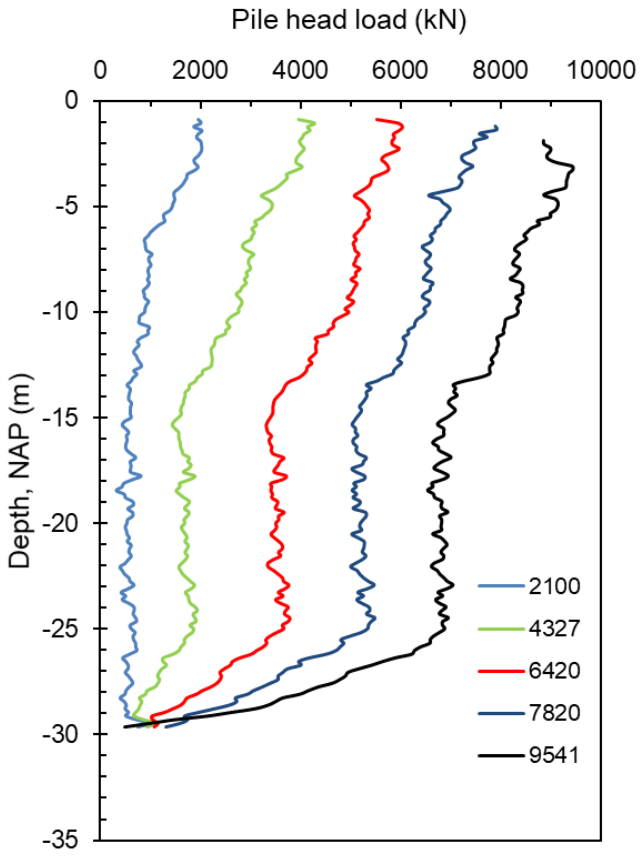

Figure 29 Load distribution with depth in MV pile test

The geotechnical capacity of the piles in the Pleistocene sand layer (below -25m NAP) was the focus of this study. The average shaft resistance, q_{st} mobilised in the sand layer is given by, the maximum shaft load at any depth, Q_s:

$$q_{st} = Q_s/\text{Area of shaft} \qquad \text{Equation 8}$$

The average q_{st} value mobilised in the Pleistocene sand layer is plotted against the average CPT q_c value along the grouted anchor section in Figure 30.

It is apparent from the Figure 30 that the limiting resistance recommended in CUR-166 was exceeded in all tests. The correlation between q_{st} value and q_c was constant and no limiting value or either q_{st} or q_c is necessary. In addition a slightly lower α_t value of 0.0125 rather than the code recommended value of 0.015 gave a much more reliable prediction of the mobilised shaft resistance. As a result the following equation was used to predict the capacity of MV piles in the numerical analyses described in this report.

$$q_{st} = 0.0125\, q_c \qquad \text{Equation 9}$$

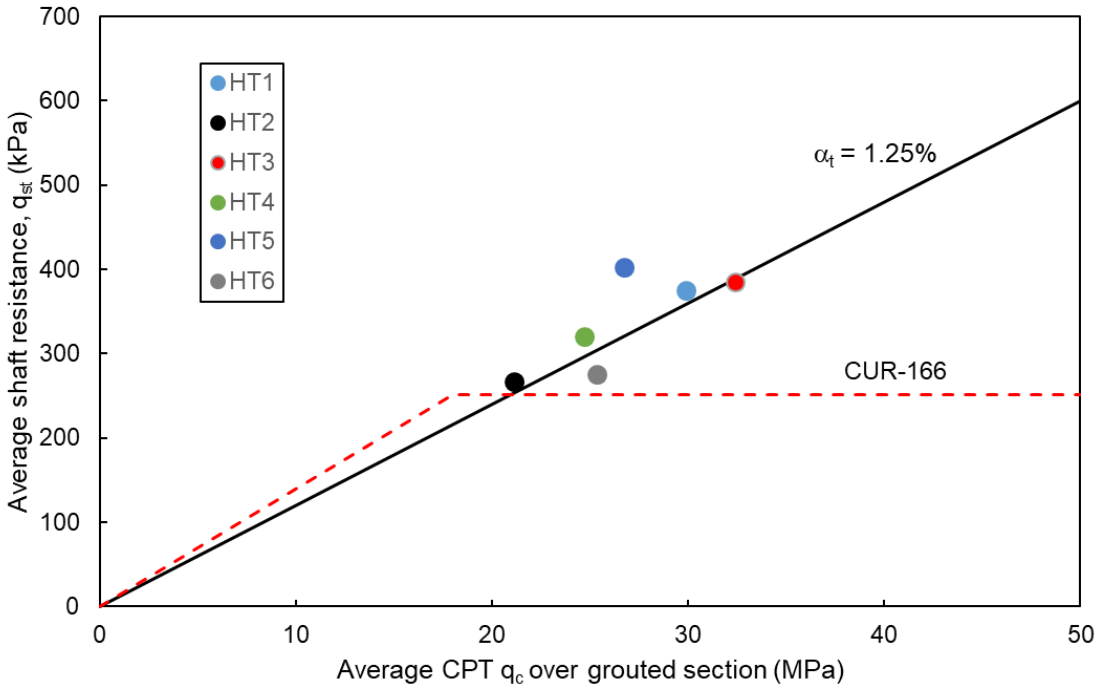

Figure 30 Average shaft resistance versus average q_c value for MV pile tests

6.3 Geotechnical Updates to the Model

A total of 4 models with updating are considered in this report, See Table 6.

A base case, Model 1 in which the soil layering and average properties described in Section 3 are modelled with the Hardening Soil model and considering the pile capacities in accordance with Dutch code procedures. In Model 2, the pile capacities are updated according to the values described in Section 4.2. In Model 3 the soil model is updated to the Hardening Soil Small Model which considers small-strain stiffness behaviour of the soil layers. Models 1 to 3 consider the construction stages of the wall. In model 4 the in-service behaviour of the wall is first considered by adding the external loads caused by cranes, storage containers etc. at the back of wall. Then a stress test is performed in which the dredge level in front of the wall is gradually increased.

Model No	Details
1	Soil layers as per Figure 24, Anchor and Pile Capacities as in Dutch Code
2	Soil layers as per Figure 14, Anchor and Pile Capacities as per Duffy et al. (2022)
3	Update of Model 2 using advanced constitutive model HSS
4	Stress Testing of Model 3

Table 6 Model updates considered in this report

7 RESULTS AND DISCUSSION

In this section the numerical results of the first 3 models are compared with the wall response measured during construction of the wall. This is achieved by comparing two principal performance indicators.

(i) Force in the MV Pile
(ii) Displacement in the combi retaining wall

The forces in the MV pile are measured using six fiber bragg grating (FBG) sensors located near the head of the pile, See Figure 31. The sensor thus measure the tension force in a single cross-section of the pile. The cross-section is located at approximately -2.3m N.A.P (Schouten 2020).

Figure 31 FBG gauges on MV Piles (Schouten 2020)

The displacements of the combi wall were measured using a standard inclinometer installed in a casing attached to the tubular piles. Whilst the FBGs readings were taken daily using a data logger, displacement measurements were only made on discrete dates during the dredging process.

7.1 Model 1

In the first model analysed the soil is modelled using the Hardening Soil model available in Plaxis and the pile capacities are modelled according to NEN 1997. In Figure 32 the measured force is compared to the force predicted using the FE model. In general there is reasonably good agreement between the shape of the measured and predicted forces, albeit the model appears to under-predict the force at the start of dredging (when the soil level in front of the wall is -5.5m N.A.P) and over-predict the force at the end of dredging.

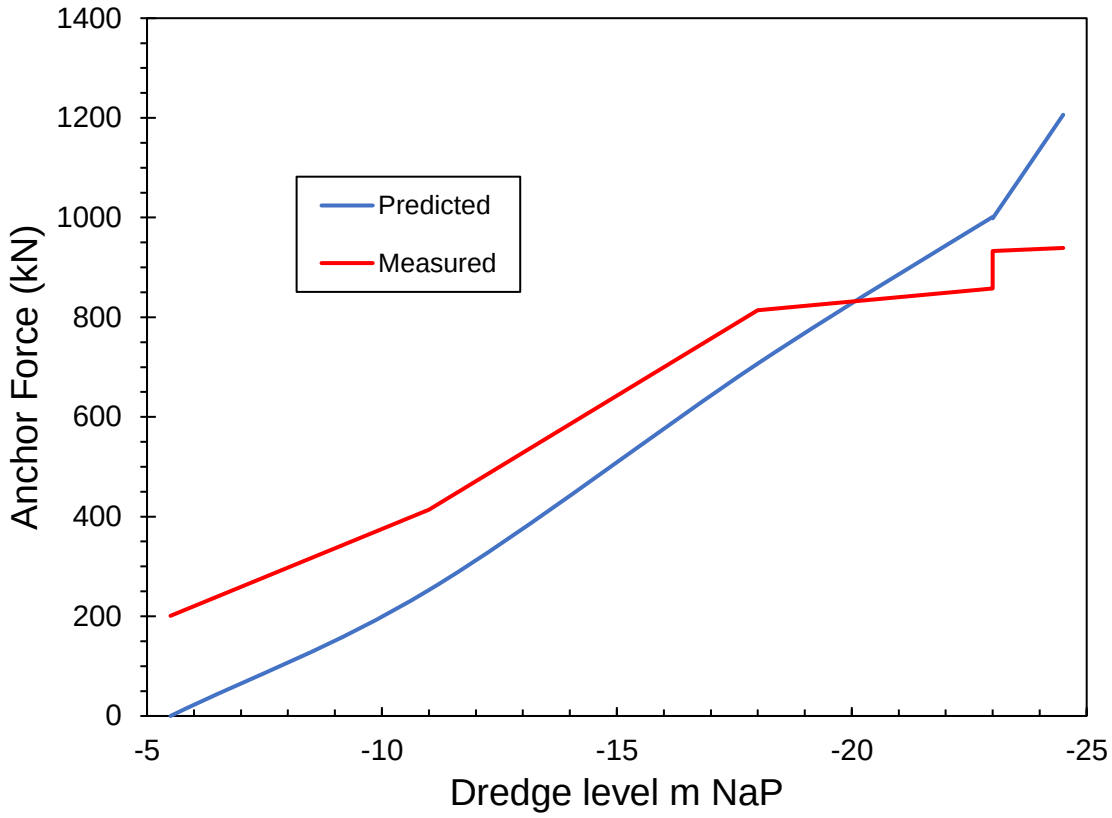

Figure 32 Measured and predicted anchor force for Model 1

Potential sources of error in the measured forces were considered. From Figure 32 the FE model predicts there is no load transfer into the anchor until dredging starts in front of the wall. The measurements indicate that a force of 200 kN is present. This force is the difference in strain between the time when the gauges were first monitored and the time to the start of dredging. It is impossible to determine if these changes in strain occurred because of loading or strain gauge drift/temperature effects etc.

Considering the purpose of the anchor is to provide additional lateral stability as dredging progresses the model (blue line) prediction of increasing load as the dredging progresses is in keeping with the expected physical response of the system. The forces would be expected to increase at a faster rate as the dredge depth increases. In contrast, the measured anchor forces initially increase as expected, however, after a dredge level of -18m N.A.P (or measured anchor force of 814 kN), the rate of increase of the measured anchor force decreases. The MV Pile (anchor) is an I-Beam with FBG

sensors located on one cross-section (near the head of the anchor), see Figure 31. FBGs were placed at three locations on the cross-section of the beam, the top and bottom flanges and the middle web. These three independent measurements of strain are shown in Figure 33. It is apparent that the force (strain) is equally distributed across the cross-section of the anchor during the initial stages of the excavation (up to around 45 days into the dredging procedure when the dredge level reached -18m N.A.P). Up to this point the force in the top, bottom and middle of the anchor were approximately equal and the average of the top and bottom sensors (Average T&B) gave a good indication of the load in the anchor. After this point the anchor experienced bending, the force in the top flange increased significantly, whilst the force in the bottom decreased. Both gauges appear to be responding to increased dredge level. However, the force measured in the web (middle) and the average of the T&B do not increase, despite the decrease in the dredge level. Therefore, it is possible that the anchor force measurements do not fully reflect the increase in force due to dredging below -18m N.A.P. due to the non-uniform strain conditions in the anchor at the level at which the measurements are made.

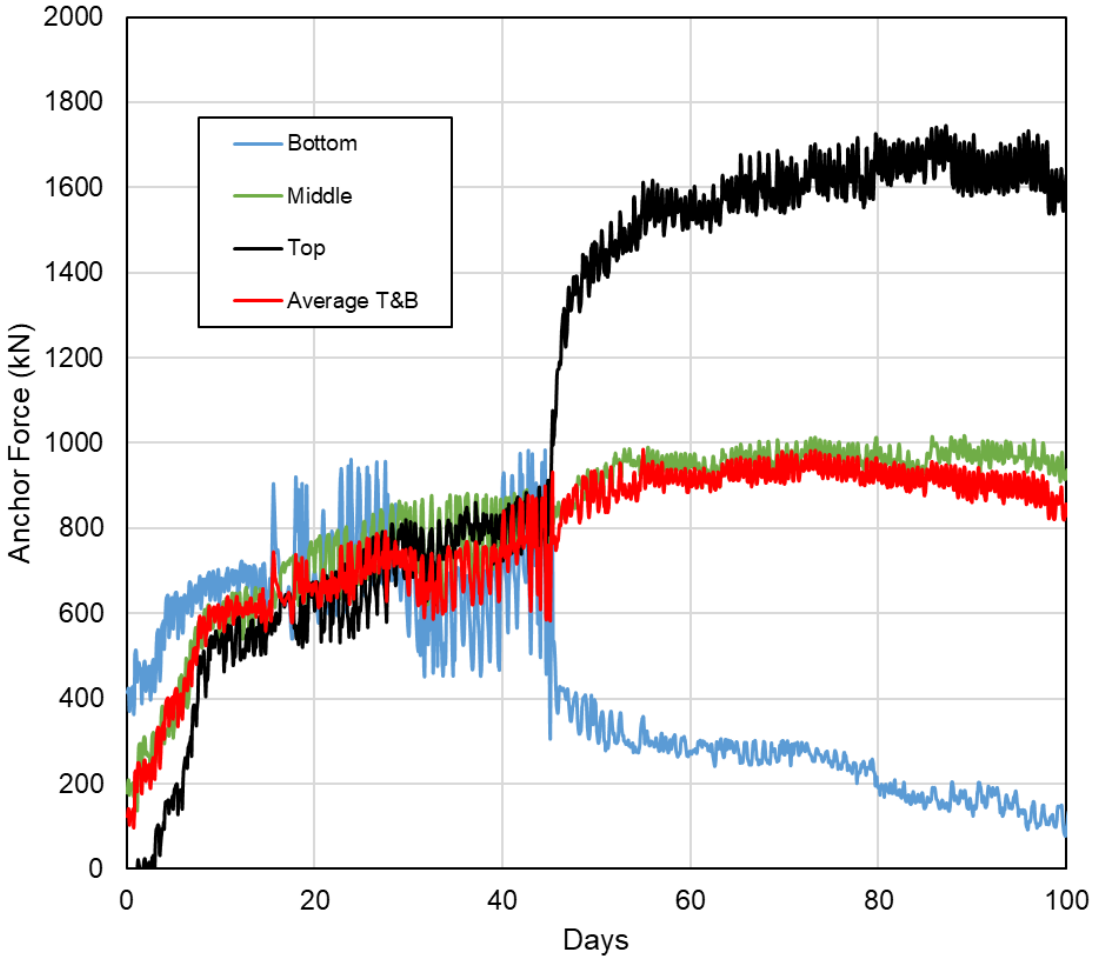

Figure 33 Axial force measured by FBG sensors on the MV Pile (anchor) over time

Although dredging operations were continuously performed for more than 100 days, measurements of the wall deflection were made only periodically during the dredging process. The measured and predicted lateral displacements of the combi wall made soon after dredging stage 4, Table 2, when the dredging level was -23m N.A.P are compared in Figure 34. Whilst the model captures deflected shape of the wall very well, the maximum predicted settlement (≈45mm) is 10 mm higher than the measured settlement at that stage of the construction process.

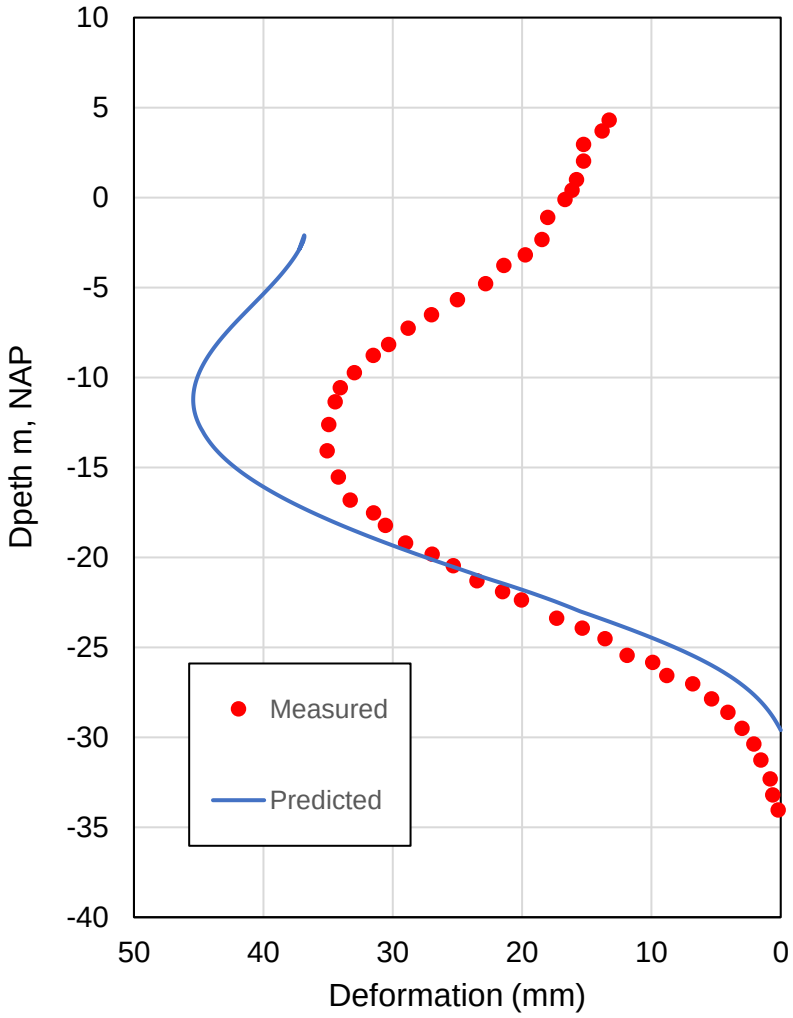

Figure 34 Measured and predicted wall displacement for Model 1 (dredging stage 4, -23 N.A.P, See Table 2)

7.2 Model 2

The second analyses, See Table 6 adopted the same soil model but updated the capacity models for the axial and anchor piles as described in Section Pile Properties6.2. The update had the effect that the forces predicted in Model 2 were slightly higher than Model 1, See Figure 35.

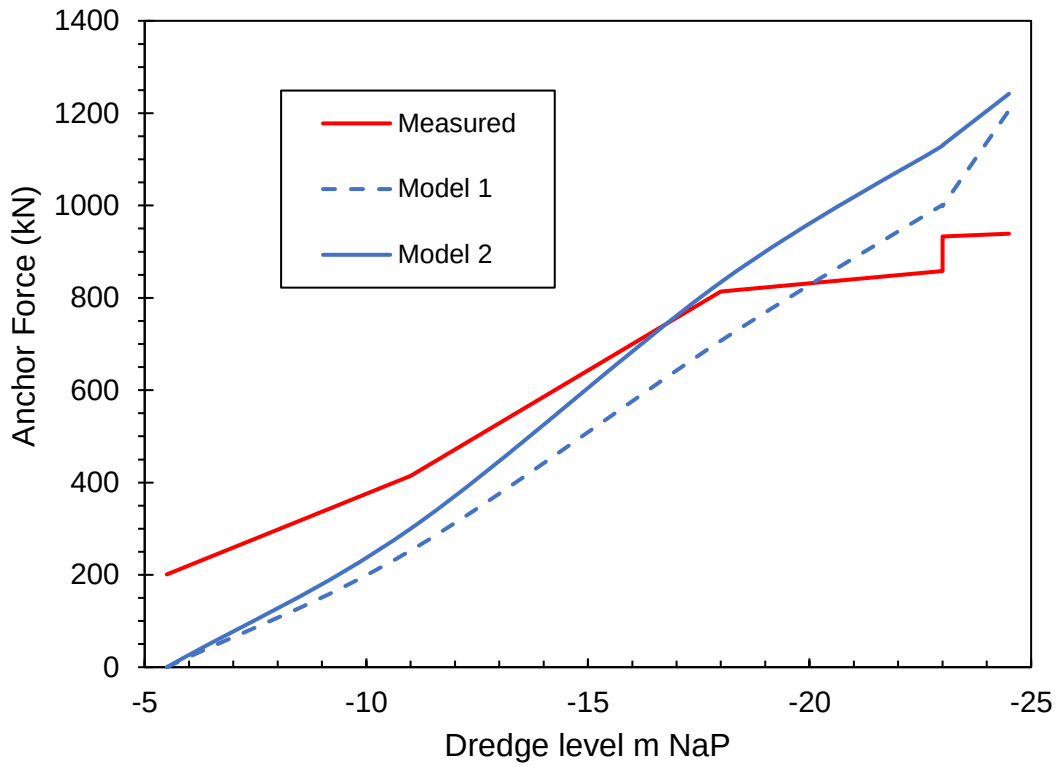

Figure 35 Measured and predicted anchor force for Model 2

The ability of the anchors to support higher loads results in slight reductions in the horizontal displacements of the combi wall required to maintain overall equilibrium, See Figure 36.

Whilst it was expected that the updated resistance of the anchors and the piles would have a significant effect on the model, the rather modest increase occurred because of two interrelated factors:

(i) Although the application of the new pile factors described in S356.2 resulted in much higher predicted pile capacities than those given by the national norm, the anchor forces predicted in the model (around 1000 kN) are less than 15% of the ultimate resistance that could be mobilised by these anchors. Thus indicating significant factors of safety against failure.

(ii) The finite element model considers the resistance of the piles to be mobilised using a simple elastic-plastic model. Plasticity occurs only the resistance is fully mobilised. Therefore, given that the anchors modelled with either the norm or the updated resistance factors were remote from failure, the response predicted was quite similar.

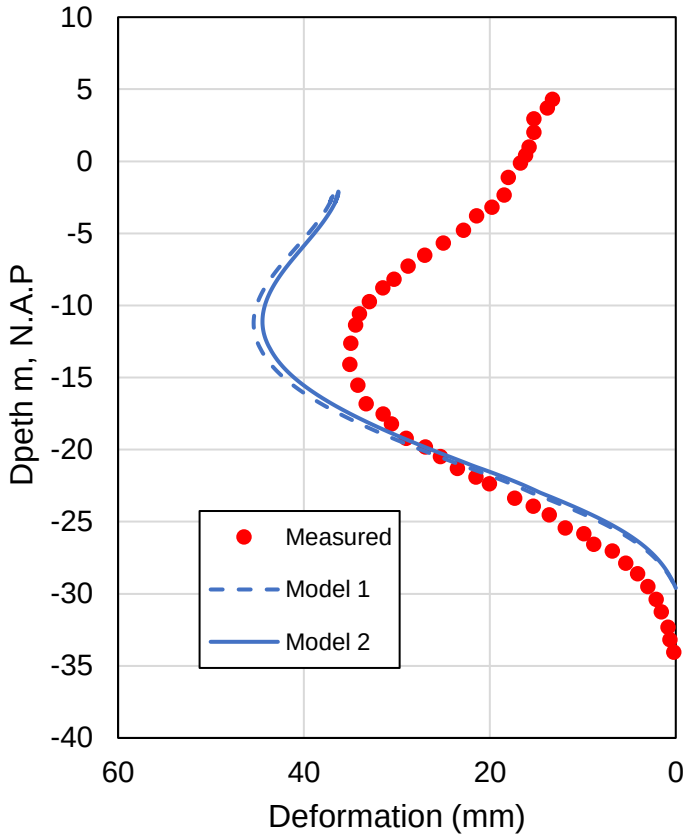

Figure 36 Measured and predicted wall displacement for Model 2 (dredging stage 4, -23 N.A.P, See Table 2)

7.3 Model 3

The third analyses, See Table 6 adopted an updated soil model together with updated capacity models for the axial and anchor piles. In this analysis the advanced form of the HS model, namely: the Hardening Soil model with Small-strain stiffness (HSS) model was adopted. The model accounts for the high-stiffness of soils at small-strain levels noted by Hardin and Drnevich (1972), Obrzud (2010), See Figure 4b, which shows that for serviceability analyses of retaining wall problems that are remote from failure, relatively high soil stiffness values are mobilised. The effect of implementing the HSS model is considered in Figure 37 and Figure 38. Whilst the anchor force shown Figure 37 is not strongly affected because of the reason given in the discussion regarding anchors forces in Model 2, the prediction of the lateral deformation of the wall in Figure 38 is much improved.

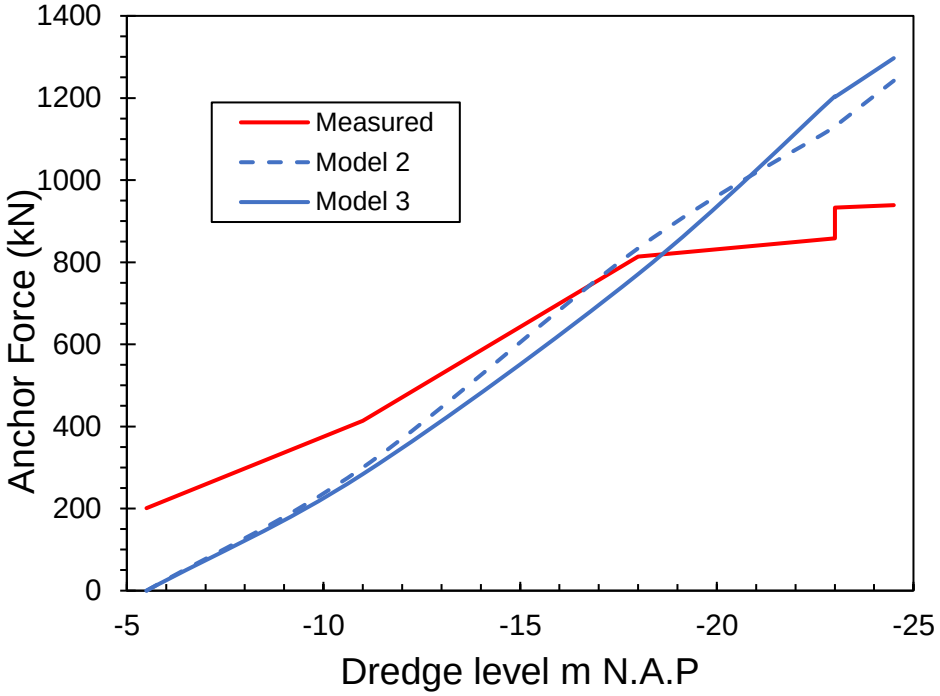

Figure 37 Measured and predicted anchor force for Model 3

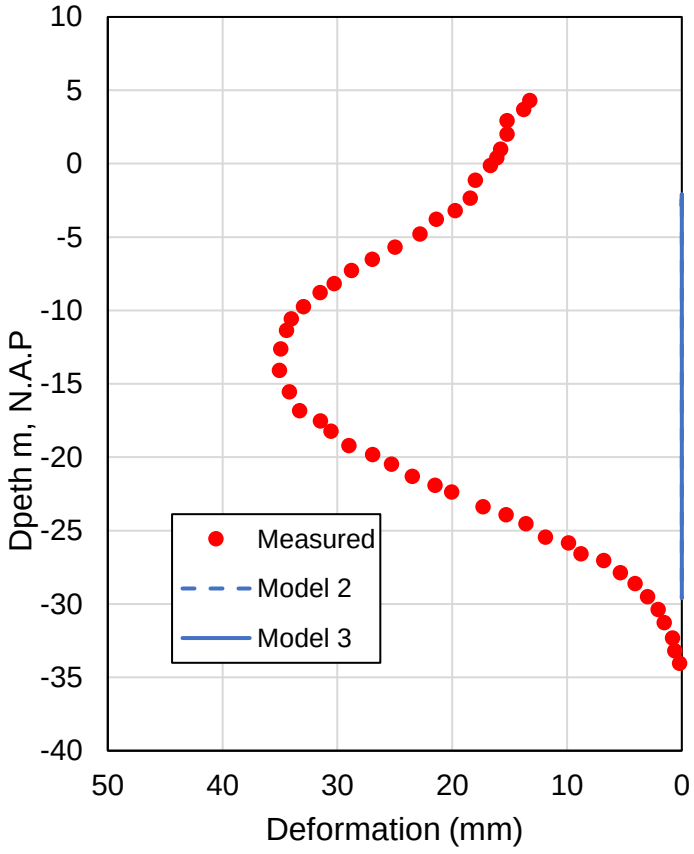

Figure 38 Measured and predicted wall displacement for Model 3
(dredging stage 4, -23 N.A.P, See Table 2)

Given the excellent performance of HSS model in predicting the lateral deformation of the combi wall when the dredge level reached -23m N.A.P, the performance of the model for a range of excavation levels (from -18m N.A.P to the maximum dredge level of -24.5m N.A.P) was assessed and the results are shown in Figure 39.

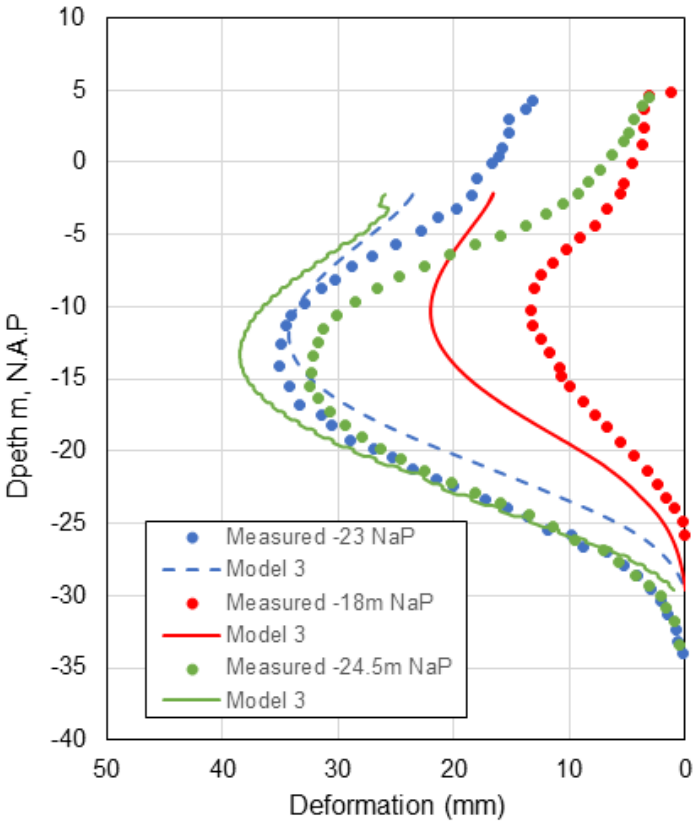

Figure 39 Measured and predicted wall displacement for Model 3, for a range of dredging depths, See Table 2.

Whilst the model appears to over-predict the lateral displacement at a dredge level of -18m N.A.P, suggesting either the soil stiffness was under-estimated or that some level of resistance was developed by the anchor (as indicated by the anchor measurements) it provided excellent predictions of lateral displacement and anchor force for the deepest dredge levels. This gives confidence that Model 3 where updating was based purely on physical mechanisms and not by parameter adjustment to obtain good-fit provides robust predictions of the behaviour of the complex soil-structure interaction problem at all stages of the construction process.

7.4 Stress Testing – Model 4

In the final modelling stage the validated model was used to:

Firstly predict the effect of adding surface loads as specified as the typical working loads for this type of quay wall

Stress testing was performed by increasing the dredge level on the seaward side of the wall. The dredge level was increased from -24.5m to -35m N.A.P, See Figure 40.

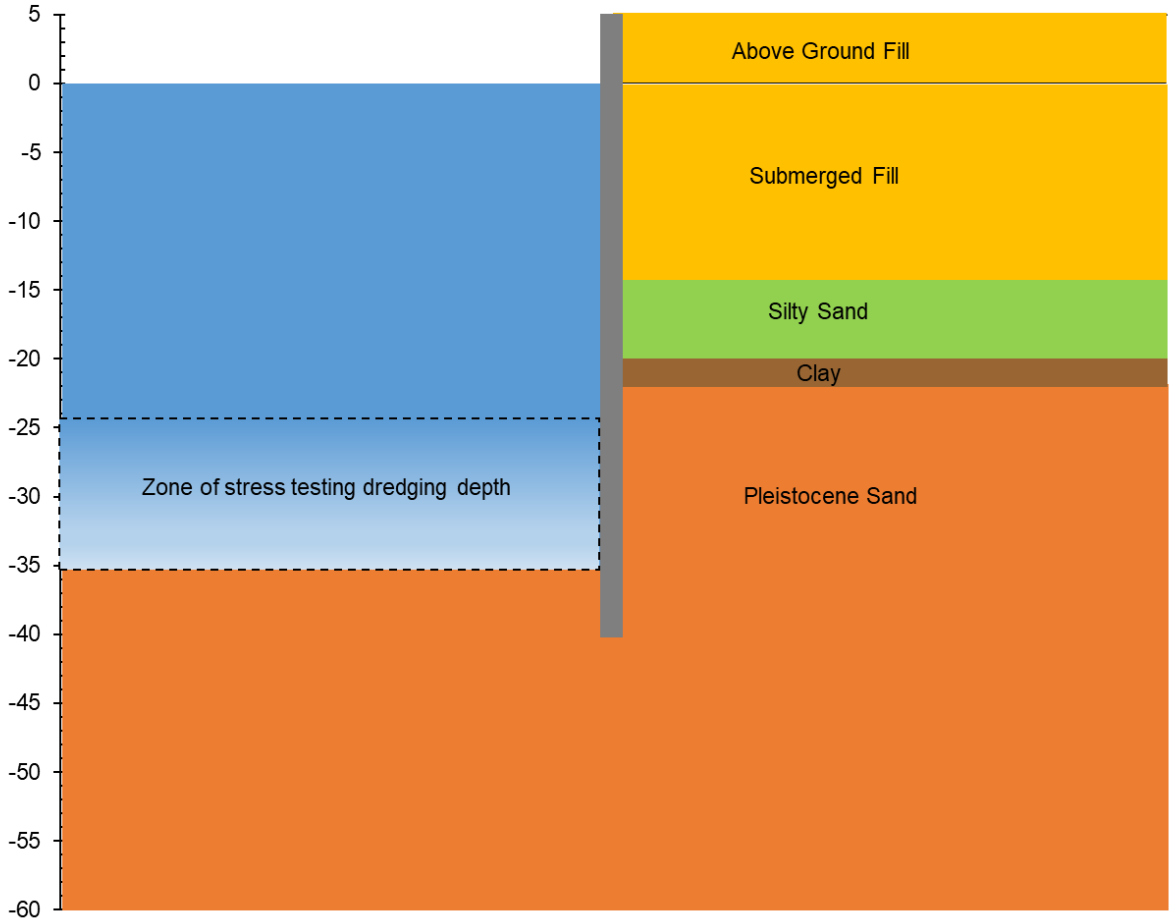

Figure 40 Stress testing to investigate the impact of dredging on quay wall response

When the construction phase is complete and the dredge level is -24.5 m N.A.P, the application of the external loading causes significant impact in the model predictions:

(i) the predicted anchor force nearly doubles from ≈ 1300 kN to 2550 kN, SeeFigure 41.

(ii) When the external load is applied the maximum wall displacement increases from 46mm to 64mm and the deflected shape changes, with the point of maximum displacement moving higher up the wall, See Figure 42.

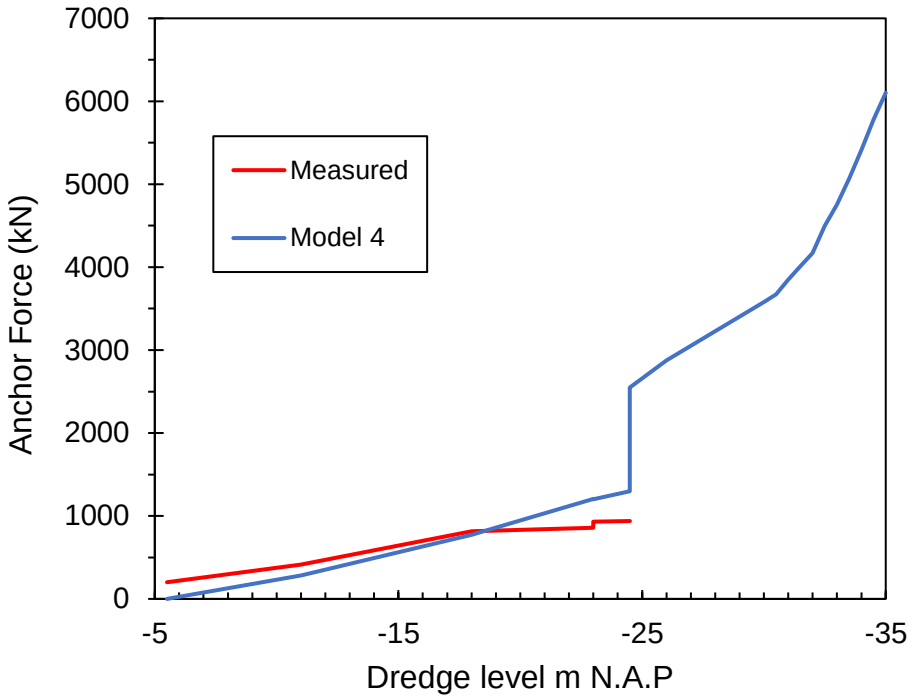

Figure 41 Stress testing of applying service loading followed by dredging from -24.5m to -35m N.A.P, impact on axial force in anchor

Increasing the dredging level had the following impacts:

(i) the anchor force predicted increased to ≈3500 kN when the dredge level increased to -30m N.A.P and to 6100 kN when the dredge level increased to -35m N.A.P, See **Error! Reference source not found.**.

(ii) The maximum wall displacement increased from 110mm to 230 mm when the dredge level increased from-30m N.A.P to -35m N.A.P, See Figure 42.

Proof load testing of MV Piles at the quay wall location has shown that the ultimate geotechnical axial capacity of these piles is ≈ 10,000 kN. Therefore at the current dredge level (-24.5m) and with the external loads applied the factor of safety of the anchors is high (10,000/2550) =3.92. It would appear that the quay wall has significant capacity to increase the draught allowing significantly larger vessels to use the facility. Increasing the dredge level to -30m (i.e. additional draught of 5.5m) would result in the factor of safety of the anchors reducing to (10000/3500) = 2.86 and the wall maximum wall displacement increasing to 110mm.

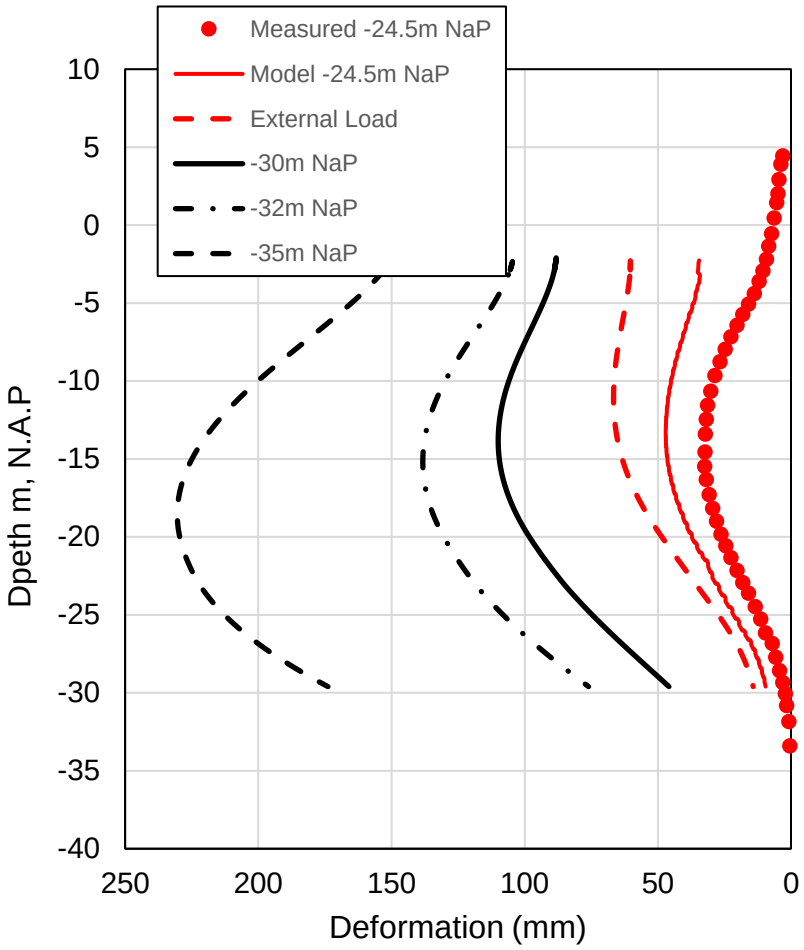

Figure 42 Effect of stress testing of applying service loading and then dredging from -24.5m to -35m N.A.P to lateral displacements

8 CONCLUSION

The deliverable considered the benefit of using digital twins to control risks associated with deep excavation projects. Having identified the role of digital twins in implementing the observational approach in risk management a detailed case of using construction records in the implementation of a deep sea quay wall was investigated.

Detailed monitoring data including wall movements coupled with forces measured in embedded geotechnical elements collected during the construction of a deep-sea quay wall coupled with updated model of the capacity of various embedded elements including tension anchors and axially loaded piles were implemented into a a finite element model to determine the safety state for a quay wall throughout the construction period. The quay wall was constructed in a geologically complex delta environment. A geological model was developed by considering the statistical variability of in-situ CPT test data. Correlations were implemented to provide strength and stiffness properties for the soil layers based on representative CPT values for each geological layer. These soil properties were implemented into advanced soil models together with updated geotechnical models for the SI and anchor piles used to provide the overall system response of the quay wall. The model allowed excellent predictions of the quay wall response during the extreme loading conditions associated with dredging during construction.

This verified model was then used to assess the impact of dredging in front of the quay wall that would allow the use of the facility for much larger vessels. The safety level of the quay wall can be quantified by tracking the tension force in the anchor pile and the displacement of the wall. Proof load testing of the anchor piles at the quay wall location has shown that the ultimate geotechnical axial capacity of these piles is ≈ 10,000 kN. Therefore at the current dredge level (-24.5m) and with the external loads applied the factor of safety of the anchors is high (10,000/2550) =3.92. The maximum lateral displacement of the wall is less than 40 mm. It would appear that the quay wall has significant capacity to increase the draught allowing significantly larger vessels to use the facility.

The analyses performed herein show that increasing the dredge level to -30m NAP (i.e. additional draught of 5.5m) would result in the factor of safety of the anchors reducing to (10000/3500) = 2.86 and the wall maximum wall displacement increasing to 110mm. Increasing the dredge level the dredge level to -35m NAP caused the factor of safety of the anchors to reduce to an unacceptably low value of 1.5 and the maximum wall displacements to exceed 200 mm.

This demonstration of digital twinning whereby an advanced finite element model and detailed monitoring data that reveal the performance of a complex structure during extreme loading demonstrated that an existing quay wall has significant additional capacity. The implication of such a demonstration project could be that the quay wall can be re-purposed for much larger vessels without the significant financial, environmental and downtime costs of replacing the main structure.

9 REFERENCES

Broos, E.J., 2010. Design & construct contract for a deepsea quay wall in the Port of Rotterdam: Case study Brammen terminal. https://repository.tudelft.nl/

Chai, F. Xue, J, Tiang, F.B. Duffy, K. and Gavin, K. (2022) The Influence of a Thin Weak Clay Layer on the Close-ended Pile Behaviors in Sand, 8th International Symposium on Geotechnical Safety and Risk (ISGSR 2022)

CUR 166 (1997) Damwandconstructies / Sheet Pile Construction, 3rd Edition, CUR, Gouda.

de Gigt, J.G., and Brasinga, H.E., (1990) Diepwaterterminal op de Maasvlakte te Rotterdam. Geotechnische aspecten zeekade en bewerkingskade, PT Civiele Techniek, 2. pp 7-13.

de Gigt, J., Kleef, V., Taneja, P., Lightringen, H., 2010. Development of container handling in the Port of Rotterdam, in: Port Infrastructure Seminar 2010. Delft, Netherlands.

Do TN, Ou CY, Chen RP (2016) A study of failure mechanisms for deep excavations in soft clay using the finite element method. Computers and Geotechnics, Vol. 73 pp 53–163.

Duffy K, Gavin, K. Korff, M, de Lange, D. and Roubos, A. (2022). Axial pile testing in very dense sand. Submitted to ASCE Journal of Geotechnical and Geoenvironmental Engineering.

Fang, W., Shao, Y. Love, P. Hartmann, T. and Liu, W. (2023). Detecting anomalies and de-noising monitoring data from sensors: A smart data approach. Advanced Engineering Informatics. Vol. 55

Gavin, K. Cadogan, D. Tolooiyan, A. and Casey, P.(2013) The base resistance of non-displacement piles in sand. Part I. Proceedings of the ICE - Geotechnical Engineering, Volume 166, Issue 6, April pages 540 –548

Gerbert, P.; Castagnino, S.; Rothballer, C.; Renz, A.; Filitz, R. The transformative power of building information modeling. In Digital in Engineering and Construction; Boston Consulting Group: Boston, MA, USA, 2016.

Hardin, B. O. and Drnevich, V. P. (1972), "Shear modulus and damping in soils: Design equations and curves", Journal of the Soil Mechanics and Foundations Division, ASCE, Vol. 98, pp. 667-692.

Hong, C., Zhang, J., & Chen, W. (2022). An Integrated Intelligent Approach for Monitoring and Management of a Deep Foundation Pit in a Subway Station. Sensors, 22(22), 8737.

Mu, L., Zhang, P. Shi, Z. Gu, Z. (2023) Predicting longitudinal tunnel deformation due to deep excavation induced ground movement, Tunnelling and Underground Space Technology, Vol. 131

Obrzud, R.F. On the use of the Hardening Soil Small Strain model in geotechnical practice. Numer. Geotech. Struct. 2010, 16, 15–32.

Phoon, K. K., J. Ching, and Y. Wang. 2019. “Managing Risk inGeotechnical Engineering – from Data to Digitalization.” In Proc. 7th International Symposium on Geotechnical Safety and Risk (ISGSR 2019), Taipei, pp 13–34.

Popielski, P.; Kasprzak, A.; Bednarz, B. Using Thermal Monitoring and Fibre Optic Measurements to Verify Numerical Models, Soil Parameters and to Determine the Impact of the Implemented Investment on Neighbouring Structures. Sustainability 2022, 14, 405

Putteman, J., Broos, E.J., Brassinga, H.E., Spruit, R., De Vos, M. and Timmermans, A.L.J., (2019). MV tension pile load tests in the Port of Rotterdam: practical aspects and geotechnical behaviour. Proceeding of the European Conference on Soil Mechanics and Geotechnical Engineering, Reykjavik, 2019

Robertson, P.K., (1990). Soil classification using the cone penetration test. Canadian Geotechnical Journal, 27(1): 151-158.

Roubos, A. A. (2019). Enhancing reliability-based assessments of quay walls. Delft, the Netherlands: Delft University of Technology. ISBN

Schanz, T., Vermeer, P. A., and Bonnier, P. G. (1999). The hardening soil model: formulation and verification. In Beyond 2000 in Computational Geotechnics-10 Years of Plaxis, Rotterdam. pp: 281–290

Schouten, O. (2022). Optimising the functionality of smart quay walls using measurement data obtained during the construction process: A case study in the port of Rotterdam: HHTT-quay. Master Thesis, TU Delft

Sun, Z., Li, H., Bao, Y., Meng, X., & Zhang, D. (2023). Intelligent Risk Prognosis and Control of Foundation Pit Excavation Based on Digital Twin. Buildings, 13(1), 247.

Vos, P. C., Bunnik, F. P. M., Cohen, K. M., and Cremer, H.: A staged geogenetic approach to underwater archaeological prospection in the Port of Rotterdam (Yangtzehaven, Maasvlakte, The Netherlands): A geological and palaeoenvironmental case study for local mapping of Mesolithic lowland landscapes, Quat Int, 367, 4-31, 10.1016/j.quaint.2014.11.056, 2015.

Westerbeke, F. (2021) Geotechnical bearing capacity of MV piles: Improving the design based on full scale load tests in the Port of Rotterdam, Master Thesis, TU Delft, https://repository.tudelft.nl/islandora/object/uuid:6f7bb64b-9dc2-4a30-85b8-8f47d1e698ea?collection=education

Yin, H.Y., and Hicher, P.Y. (2018) Chapter 5, Multi-Scale Modeling of the Mechanical Behaviour of Clays, Editor(s): François Nicot, Olivier Millet, Advances in Multi-Physics and Multi-Scale Couplings in Geo-Environmental Mechanics, Elsevier, pp 133-169,